SLAC-PUB-1737
April 1976
(T/E)

THE PRODUCTION OF NEW PARTICLES AND MUON-ELECTRON EVENTS IN e^+-e^- ANNIHILATION AT SPEAR*

B. Richter

CERN, Geneva, Switzerland

and

Stanford Linear Accelerator Center
Stanford University, Stanford, California 94305

(Review paper presented at the Discussion Meeting of the Royal Society on "New Particles and New Quantum Numbers," London, England, 11 March 1976. To be published in Proceedings of the Royal Society.)

*Work supported in part by the Energy Research and Development Administration.

I. INTRODUCTION

It is about 18 months since the discovery of the first ψ particle at SPEAR[1] and at BNL.[2] During this time, the e^+e^- colliding-beam experiments have found a huge amount of new information on this new layer of hadron structure: nine states with widths ranging from tens of keV to many MeV, the principal decay modes and quantum numbers of some of the states, limits on charmed-particle production, μe events, etc. There is too much to review in a single talk, so I shall limit my discussion to the new states, the total hadron cross section, and the μe events. The work that I shall discuss has been done by the SLAC/LBL magnetic detector group at the SPEAR e^+e^- storage ring of the Stanford Linear Accelerator Center.

II. APPARATUS

The apparatus consists of two parts: the storage ring and the detector. Much more than at conventional accelerators, the machine itself is coupled to the apparatus, and the properties of the machine are intimately connected to the resolution of the detector. The SPEAR ring[3] is a single ring in which one bunch of electrons and one bunch of positrons circulate in opposite directions in a common vacuum chamber, colliding only at the centers of the two experimental areas. The center-of-mass energy E^* of the e^+e^- system is at present variable from 2.6 GeV to 7.8 GeV. The lower limit comes from the control system and the upper limit from the rf drive power available to the final high-power amplifiers. Modifications to the rf have been made, and the ring should soon be able to operate at its maximum design energy of $E^* = 8.6$ GeV.

The electron and positron bunches in the ring are quite small, having a size (gaussian standard deviation in x,y,z) of about 0.1 cm x 0.01 cm x 5 cm. The short bunch length gives about an 0.2-nsec collision time, providing a well-defined start signal for time-of-flight particle identification systems. The energy spread in the beams is proportional to the (beam energy)^2 with $\sigma(E^*) = 0.8$ MeV at 3 GeV.

An exploded view of the SLAC/LBL magnetic detector is shown in Fig. 1. It is a large solenoid magnet with a coil about 3 meters in diameter and about 3-m long. The coil is coaxial with the beam direction, and the e^+e^- collision point is at the center of the magnet. The magnetic field is about 4 kilogauss.

Figure 2 is a view along the axis of the solenoid at the center of the coil. The beam direction is perpendicular to the plane of the figure. A particle produced in an e^+e^- interaction as it travelled out from the collision point would encounter the 0.15mm stainless steel vacuum chamber; 2-8 mm thick cylindrical scintillation counters; two cylindrical proportional chambers (not shown in the figure); 4 cylindrical magnetostrictive spark chambers, each with 4 planes having wires at $\pm 2^\circ$ and $\pm 4^\circ$ with respect to the field direction; one of 48 2.5-cm thick scintillators used in the trigger system and in a time-of-flight system for particle identification; the one-radiation-length thick aluminum magnet coil; one of 24 Pb-scintillator shower counters used for electron and photon identification; the 20-cm thick steel return yoke of the magnet; and finally 2 layers of magnetostrictive spark chambers used for muon identification.

The momentum resolution for a charged particle is about $2\% \times P$ (GeV/c) at 90°. The trigger solid angle is about $0.65 \times 4\pi$ ($50^\circ < \theta < 130^\circ$), while the solid angle over which particles can be tracked is somewhat larger ($0.75 \times 4\pi$). The trigger requires ≥ 2 charged particles in the trigger solid angle.

The time-of-flight system is capable of separating π from K (3σ) up to about 600 MeV/c, and K from p up to about 1.1 GeV/c. The shower counters have a fractional energy resolution for electrons or photons of about 25% (σ) at 1 GeV.

The apparatus is large and so is the group which built it and has done these experiments. The group is a collaboration of SLAC and LBL physicists who have all worked hard on different facets of the apparatus and the analysis. Their names are listed in Ref. 4.

III. THE ψ AND ψ'

Electron-positron annihilation takes place in the state with the quantum numbers of one photon, $J^{PC} = 1^{--}$, strangeness, baryon number and charge all equal to zero. Any particle coupled to the photon with these quantum numbers can be observed as an enhancement in the total annihilation cross section when the energy in the e^+e^- system equals the mass of the state. The state is detected, of course, by observing its decay products.

Figure 3 shows the total observed hadron production cross section as a function of energy. The only features that stand out when the data are plotted on this scale are enormous peaks at the mass of the $\psi(3.1)$ $[\psi(3.1) \equiv \psi]$ and $\psi(3.7)$ $[\psi(3.7) \equiv \psi']$ which were discovered last November. The peak cross section observed is not the true peak cross section for the ψ and ψ' have widths much narrower than the energy spread of the e^+e^- system:

$$\sigma_{obs} \approx (\Gamma_R/\Delta E_\gamma)\sigma_{true} \quad . \tag{1}$$

Equation (1) gives the rough relation between the observed and true peak heights for a resonance with a width Γ_R which is much narrower than the energy spread ΔE_γ in the beams.

The energy spread in the beams is determined by quantum fluctuations in synchrotron radiation and by the interaction of the circulating beams with the electromagnetic fields generated by their passage through the vacuum chamber. This energy spread depends on the current in each beam and cannot be absolutely determined with any great precision. The observed area under the Breit-Wigner resonance, however, does not depend on the energy spread in the beams, and this is the method we used to determine the widths of the two resonances. This area is given by

$$\int \sigma_i \, dE = \frac{2\pi^2}{M^2} (2J + 1) \frac{\Gamma_e \Gamma_i}{\Gamma} , \tag{2}$$

where J is the spin of the resonance, M is the mass, Γ_e is the partial width to e^+e^-, Γ_i is the partial width to the final state being observed, and Γ is the total width. The widths resulting from this method[5,6] of analysis are given in Table I. The width of the ψ is about 69 keV, while that of the ψ' is 225 keV. These widths are about a factor of a

thousand down from the widths we might expect of normal hadron resonances of these masses.

In the width analysis we assumed that both ψs have $J^{PC} = 1^{--}$, which are the quantum numbers of the one-photon intermediate state presumed to be involved in ψ production. While this is the most likely assignment, others are possible, and, indeed, in the early days after the discovery of these particles, other quantum numbers were considered. The J^{PC} assignment can be checked experimentally by looking at the interference of the resonance with the non-resonant quantum-electrodynamic production of muon pairs. Only a 1^{--} state gives an effect on the rate. A 1^{+-} state, for example, would give no effect on the rate but would generate a front/back assymmetry that changed sign as one passed through the resonance.

Figure 4 shows the ratio of μ-pair production to Bhabha scattering as the storage-ring beam energy is varied through the resonance. The Bhabha scattering is dominated by t-channel exchange and interference effects would be very small. The data for both ψ and ψ' show a destructive interference below the resonance and an enhancement above the resonance as expected for a 1^{--} state. Figure 5 shows the front/back asymmetry $[(F - B)/(F + B)]$ passing through the resonance. There is no sign of any interference effect in either ψ or ψ', and we can conclude that any axial vector contribution is very small.

Table II shows the decay branching fractions to various final states of the ψ as measured by the SLAC/LBL group. Almost all of the results in this table come from data taken before September 1975. Only the $p\bar{p}$ and $p\bar{p}\eta$ branching fractions include any analysis of the new data. The relative strengths of various decay channels can be used to determine whether the ψ respects a quantum number that we know to be good only in strong interactions: that of G-parity. The analysis is complicated by the second-order electromagnetic decay of the ψ that produces the e^+e^-, $\mu^+\mu^-$, and part of the hadron final states, for this electromagnetic production of

hadrons in ψ decay is not expected to respect the G-parity quantum number. This electromagnetic hadron production, however, will produce the same ratio of hadrons to μ-pairs on the ψ resonance as off the ψ resonance ("A photon's a photon for all that"). If G-parity is a good quantum number, however, the direct pion decay modes of the ψ will produce more of an odd number or an even number of pions, depending on the G-parity. In Fig. 6 the ratio of the ratio of hadron to μ-pair production on resonance to the same ratio off-resonance is plotted vs the number of pions in the final state. We see that it is unity for the 4- and 6-pion final states, and much greater than unity for the 3-, 5-, and 7-pion final states. This indicates that the 4- and 6-pion final states are consistent with the second-order electromagnetic decay to hadrons, and that the direct hadronic decays of the ψ go preferentially to $G = -1$ states. Since the ψ obeys a strong-interaction selection rule, we not only get the G-parity but can conclude that the ψ is most probably a hadron, and can then determine its isotopic spin by looking at various other decay modes. For example, the $\Lambda\bar{\Lambda}$ decay mode would indicate an I spin = 0, as would the observation that in the $\rho\pi$ decay mode all charged states of the ρ are equally probable.[7]

Much less is known about the ψ' decays in spite of there being considerably more ψ' events to work with in our data sample than ψ events. The ψ' has much smaller branching fractions to states that are easily identified by the SLAC/LBL magnetic detector than does the ψ. The measured branching fractions are given in Table III. The principal decay mode is $\psi' \rightarrow \psi\pi\pi$. The ratio of $\pi^+\pi^-$ to $\pi^0\pi^0$ in this decay mode is 2:1, indicating that the ψ' also has $I = 0$ and $G = -1$. The branching fraction to the state $\chi(3410)$ is included here for comparison and will be discussed later on.

There has been much discussion of the so-called "missing" decay modes of the ψ'. Before discussing what they might be, we must first

define "missing." The total width of the ψ' is 225 keV. The decays to $\psi + X$, $\mu^+\mu^-$, e^+e^-, $\gamma\chi$, and the second-order electromagnetic decays to hadrons, account for 154 ± 19 keV of this total, leaving 71 ± 19 for other channels. This remainder is close to the hadronic width of the ψ, so that one might assume that the "ψ-like" hadronic decay modes of the ψ' account for the rest. We can check this assumption by comparing one of the measured hadronic channels in both the ψ and the ψ'. The largest single hadronic channel of the ψ is the $4\pi + \pi^0$ mode which has a Γ of 2.5 ± 0.6 keV. In the ψ' this mode has a Γ of 0.8 ± 0.3 keV. If this mode is used as a monitor for the "ψ-like" hadronic decays of the ψ', we can scale the observed Γs to determine the total ψ-like hadronic width of the ψ' as follows:

$$\Gamma(\psi' \to \text{hadrons "}\psi\text{-like"}) = \frac{\Gamma(\psi' \to 4\pi + \pi^0)}{\Gamma(\psi \to 4\pi + \pi)} \Gamma(\psi \to \text{hadrons}) \qquad (3)$$

Using this scaling, we find that $\Gamma(\psi' \to \text{hadrons "}\psi\text{-like"}) \approx 15$ keV, and the part of the width unaccounted for is

$$\Gamma(\psi' \text{ "missing"}) = 56 \pm 21 \text{ keV}. \qquad (4)$$

This remainder must include non-ψ-like hadronic decays of the ψ' and decays to other states lying below the ψ' mass. Note that we have already included in this analysis the decay to the $\chi(3410)$ state and that part of decays to all other states where the intermediate state decays via γ emission to the ψ.

IV. THE SEARCH FOR OTHER NARROW STATES

We have now completed a search for other narrow resonances over almost all of the mass region accessible to SPEAR.[8] The technique used is slowly to

sweep the energy of the ring and look for enhancements in the yield of hadrons. In practice, the ring energy is held constant for a minute or two while data are taken. The e^+ and e^- beam energies are then increased by about 1 MeV each, and data are taken again for one-two minutes, etc. The data are analyzed by the SLAC 370/168 computer system in real time and the cross section for one step is sent back to us while the machine energy is being changed to the next step. This technique is most sensitive to narrow resonances.

Figure 7 shows the result of the scan from the ψ mass to 7.7 GeV. The only statistically significant structure seen is the ψ' at 3.7 GeV (this technique was used to find the ψ'). The sensitivity of the scan depends on the width of a resonance and on its mass for the energy spread in the electron-positron system depends on the beam energy. The limit on the area of a resonance less than about 10-20 MeV wide (90% confidence) is given as a function of the resonance mass in Table IV. (For comparison, the area under the ψ is about 10^4 nb-MeV.) These limits increase as the width increases above 10-20 MeV, and other techniques are better used to search for states wider than about 20-30 MeV. As we shall see, states of width 30-60 MeV exist with areas less than the limits of Table IV, and this search will therefore have to be redone with increased sensitivity.

Recently, Lederman has discussed at the 1976 New York meeting of the APS, and the Columbia-FNAL-Stonybrook group has issued a preprint[9] on, the possible resonance in the e^+e^- system with a mass of 5.97 GeV. This group studied the reaction

$$p + Be \longrightarrow e^+ + e^- + X \,, \qquad (5)$$

where the e^- and e^+ were detected in two magnetic spectrometers using lead glass to identify the $e^\pm$. They found 12 events clustered within their resolution ($\sim$150 MeV FWHM) at a mass of 5.97, and estimated the background to be 3 or 4 events in this region. The group states that the odds on this being a statistical fluctuation are about 1:50.

We have made a high-statistics scan of this region with the SLAC/LBL magnetic detector at SPEAR. Because the absolute mass calibrations in different laboratories are difficult to transfer, we widened the search region to cover the mass range from 5.7 to about 6.1 GeV. No significant enhancement of hadron production was found in this region, and the 90%-confidence upper limits on the area and electronic partial width of any such state are

$$\int \sigma \, dE < 40 \text{ nb-MeV}, \tag{6a}$$

$$\Gamma(e^+e^-) < 75 \text{ eV}. \tag{6b}$$

These limits are for a narrow state less than about 20 MeV wide. The analysis to determine the limits on wider states is in progress. Note that this state cannot be wider than about 100 MeV and still be consistent with the observation of the CFS group that all events were within their resolution.

For comparison, the ψ has an area of 10^4 nb-MeV and a $\Gamma(e^+e^-)$ of 4.8 keV. We can conclude that if this possible state at 6 GeV be a 1^{--} state, the coupling to the e^+e^- system is anomalously small. Alternatively, it might have quantum numbers different from 1^{--}.

V. THE TOTAL CROSS SECTION AND THE WIDE 1^{--} STATES

Figure 8 shows the total cross section for hadron production excluding the ψs, and after radiative corrections. The errors shown are statistical with about a 10% systematic uncertainty added in quadrature. In addition, there is an overall normalization uncertainty of about 10%, and there can be a further smooth variation in the relative cross sections from the lowest to the highest energy of about 15% (from slow model-dependent changes in the detection efficiency). The cross section, except for the region around 4 GeV, shows a smooth decrease from about 30 nb at 3 GeV to about 7.5 nb at 7.8 GeV. The region around 4 GeV shows a complex structure.

The more familiar ratio R of the total hadron cross section to the μ-pair production cross section is shown in Fig. 9. The ratio R shows two plateau regions: one where $R \approx 2.5$ below 3.8 GeV, and the second above 5 GeV where $R \approx 5.2$. In the region around 4 GeV there is a complex structure with multiple peaks that is undoubtedly related somehow to the transition between the two plateau levels.

This transition region is shown in more detail in Fig. 10. The open circles are our previous data,[10] while the black points are more recent data (as of the Lepton-Photon Conference in August 1975). The new data give quite a different impression from the old. What was a single broad resonance at 4.15 GeV now seems to have a narrower compansion at 4.4 GeV and shows signs of more structure at 3.95 GeV.

We have taken further data in this region recently, and the results are shown on a more expanded scale in Fig. 11. What might have been a statistical fluctuation at 3.95 GeV before is now clearly seen to be some kind of a state, and the 4.4-GeV resonance is confirmed. There may be still more structure in this region, and considerably more data will be required to settle the question.

The widths and areas of the states in this region are very difficult to obtain quantitatively. There are three reasons for the difficulty. First, all of this rapid cross-section variation is taking place in a single angular-momentum channel, the $J^{PC} = 1^{--}$ state. The resonances may interfere with each other. Second, the transition between the low-energy and high-energy plateau regions indicates that new channels are opening in this region. It is well known that threshold effects can badly distort the shape of a classical Breit-Wigner line. Third, the shape of "background" in the transition region is not well known. The separation of the cross section into "background" and "resonance" contributions is difficult, and line shapes can be further complicated by interference with the background.

The masses, widths, areas, and couplings to the e^+e^- system of the 1^{--} states are summarized in Table V. The properties of ψ and ψ' are well determined, but the widths and areas of the other three states are uncertain by 50%. In particular, I have assumed that the 4.1-GeV region is a single state, which is by no means sure. What is clear is that a least five 1^{--} states exist, and that the widths of the three states above the beginning of the transition region in R are about 1000 times wider than those of the two below that transition region.

In the next few months, we will go over this region with smaller energy steps and better statistics to determine if still more states exist. A study of Fig. 9 will convince you that there is no large energy span sufficiently well mapped to exclude either more 20-50 MeV wide states like the 4.4, or even more small, very narrow ones.

VI. OTHER NEW STATES

In addition to the $J^{PC} = 1^{--}$ states described above, at least four other states, all with C = +1, have been found in decays via one-photon emission from the $\psi(3.7)$ or $\psi(3.1)$. Three of these states with masses between ψ and ψ' have been seen at SPEAR by the SLAC/LBL group.[11,12] One of these three states has also been seen by the DASP group,[13] and in addition another state slightly below the mass of the ψ has been found by the DASP group and the DESY-Heidelberg group.[14] In this section, I shall review the evidence of the SLAC/LBL group and summarize our knowledge of the number, widths, quantum numbers, and decay modes of these states.

The first published attempt to observe monochromatic γ-ray lines emitted in ψ' decay to other possible narrow states was by the Hofstadter group[15] working at SPEAR. Using large NaI crystals, they set an upper limit of $\approx$ 3-8% (depending on the γ energy) on the branching fraction of the ψ' to a γ-ray and a narrow state. The SLAC/LBL group has extended

this search by using the SPEAR magnetic detector as a kind of pair spectrometer. Photons produced at the interaction point can convert in the beam pipe (0.011 radiation length), one of the two trigger counters around the beam pipe (0.016 radiation length each), or in one of the two multi-wire proportional chambers around the trigger counters (0.004 radiation length each). The minimum transverse momentum of a particle to allow successful tracking in the chambers is 55 MeV/c, and both members of a pair must be seen for the γ-ray to be identified. The detection efficiency is complicated, for it depends on the number of other particles in the final state. For example, given two charged particles that trigger the apparatus, a photon can be detected if it converts anywhere up to the last proportional chamber, and in this case the γ-ray detection efficiency arises rapidly from zero at p_T = 110 MeV/c. If the members of the pair must trigger the detector, the photon must convert before the last trigger counter, and the minimum detectable p_T for a photon in this case is 200 MeV/c. The detection efficiency is shown in Fig. 12. The γ-ray energy resolution in this method is about 8 MeV(σ) at a photon energy of 200 MeV.

Figures 13a and 13b show the γ-ray spectra observed in ψ' and ψ decays, respectively. A clear peak consistent with the resolution is seen in ψ' data, and this peak corresponds to a state χ with a rest mass of 3.41 GeV. No strong peaks are observed in the ψ-decay data. Note that other states seen in ψ' decay and discussed later, would have a γ-ray transition energy lower than that of the 3.41-GeV state and would lie on the rapidly-varying region of the detection efficiency, and would be hard to see. The branching fraction of the ψ' to $\chi(3.41)$ is

$$\frac{\Gamma(\psi' \to \gamma + 3.41)}{\Gamma(\psi' \to \text{all})} = \begin{cases} 7 \pm 3\% & \text{(isotropic)} \\ 8.5 \pm 3\% & (1 + \cos^2\theta) \end{cases}, \qquad (7)$$

where the two numbers correspond to an isotropic or $(1 + \cos^2\theta)$ angular distribution of the photon; which of these two angular distributions is appropriate depends on the quantum numbers of the two states. There is too

much background under the γ-ray peak in the inclusive spectrum to allow a direct experimental determination of the angular distribution.

The 99% confidence upper limit for a γ-ray of energy corresponding to the transition to the 3.41-GeV state is given in Ref. 15 as 6%. This upper limit is below our measured branching fraction and so is not consistent with our results. The limit of Ref. 15, however, depends on the mean π^0 multiplicity assumed in the ψ' decay. The 6% limit corresponds to an assumed mean π^0 multiplicity of 2. The authors state that a higher mean π^0 multiplicity would raise their limit: a mean π^0 multiplicity of 3, for example, increases it by 30%. Using a mean π^0 multiplicity of 3, therefore, the limits of Ref. 15 would not be inconsistent with our data.

The data taken at the ψ can give an upper limit on its branching fraction to decay by γ-emission to the state $X(2.8)$ found by the DESY groups. The 90% confidence upper limit on this branching fraction is

$$\Gamma(\psi \to \gamma + X)/\Gamma(\psi \to \text{all}) < 7\% . \qquad (8)$$

The SLAC/LBL and the DASP groups looked not only for the γ-ray lines but also for the decay products of the intermediate state, which allows a more sensitive search. Data on the first state were presented by DASP, who named it P_c.[13] The SLAC/LBL group has published the results of our work on this state, which has a higher statistical accuracy.[12] Our experiment studies the decay

$$e^+ + e^- \to \mu^+ + \mu^- + X \quad , \qquad (9)$$

where the energy of the e^+e^- system is equal to the ψ' mass. The μ-meson momenta are measured in the magnetic detector and the invariant mass of the $\mu^+\mu^-$ system is determined. A large fraction of the dimuons have the mass of the ψ and these events include such decay modes as

$$\psi' \to \pi^+\pi^-\psi \qquad (10a)$$

$$\to \pi^0\pi^0\psi \qquad (10b)$$

$$\to \eta\psi \qquad (10c)$$

$$\to \gamma\gamma\psi \qquad (10d)$$

A typical $\mu^+\mu^-$ mass distribution is shown in Fig. 14.

We look for the decay mode (10d) by three different methods. In the first, both γ-rays are detected using the shower counters in the magnetic detectors. This proves the existence of the decay mode but does not have very good mass resolution. Also, the efficiency calculations are sufficiently complicated that it is difficult to determine an accurate branching fraction. In the second method, an e^+e^- pair is detected coming from the conversion of one of the two γ-rays in the beam pipe or the first trigger counters. This gives a very good energy resolution and hence a more accurate mass of the intermediate state. The statistical accuracy is low, however. In the third method, no γ-ray is detected. The missing mass distribution recoiling against the dimuon system is measured and corrected for processes such as those in Eq. (10b) and (10c). This method gives the best branching fraction.

In the first method, the γ-rays are detected by the shower counters that lie in a circle of ~1.8-meter radius just outside the aluminum coil of the magnet. The γ-ray position in the counter is determined to an accuracy of 20 cm (σ) from the relative pulse heights measured at each end of the counter and the known optical attenuation length along the counter. From the measurement of the μ momentum and the γ-ray directions, a 2C fit can be made. Figure 15 shows the resulting mass distributions of the $\psi\gamma$ system. Two solutions exist for each event, for one does not know a priori which γ-ray comes from the decay of the intermediate state. The two peaks in the graph come from this ambiguity and do not indicate the existence of two states. The solid curve shows the distribution expected from a single narrow state with a mass of roughly 3.5 or 3.27 GeV. The dotted curve shows the expected contribution from the $2\pi^0$ decay mode of the ψ' to the ψ where only two of the four γ-rays from π^0 decay are detected. The dashed curve shows the expected mass distribution if two photons are emitted by the ψ' distributed according to invariant phase space with no narrow state present.

Figure 15 demonstrates the existence of at least one state with a mass of 3.5 or 3.27 GeV. The width is consistent with the resolution, which for this method is about 80 MeV full-width half-maximum (FWHM). The state at 3.4 GeV does not show up strongly in this decay mode.

Figure 16 shows the $\gamma\psi$ mass when one of the two γ-rays converts in the beam pipe or first counter. The resolution is much improved (30 MeV FWHM). The events cluster around a mass of 3.5 or 3.28 GeV.

Figure 17 shows the missing mass spectrum recoiling against the ψ (unshaded). The shaded region shows the distribution after subtracting half of the acceptance-corrected mass distribution from the reaction (10a). This removes the π^0 contribution to the spectrum from (10b) for the ψ' has I spin = 0. This can be done accurately for the dimuon acceptance of the reactions (10a) and (10b) are identical. The dashed line in the figure shows the contribution of the direct radiative μ-pair

production

$$e^+e^- \to \mu^+\mu^-\gamma \quad . \tag{11}$$

The peak at ~0.3 GeV^2 is from the decay $\psi' \to \eta\psi$.

After subtracting $2\pi^0$ contribution, the radiative contribution, and cutting out the region of the η, we find

$$\frac{\psi' \to \gamma P_C}{\psi \to \text{all}} \cdot \frac{P_C \to \gamma\psi}{P_C \to \text{all}} = 3.6 \pm 0.7\% \quad . \tag{12}$$

The Hofstadter group's limit on monochromatic γ-rays of an energy corresponding to transition from ψ' to P_C is 7% (9% with the higher π^0 multiplicity). This result, together with our measurement of the cascade branching fraction, can give a lower bound to the fraction of P_C decays that go to the ψ by γ-emission. This bound is

$$\frac{\Gamma(P_C \to \gamma + \psi)}{\Gamma(P_C \to \text{all})} > \frac{3.6 \pm 0.7\ \%}{7\%\ \ (9\%)} = 50\%\ \ (40\%) \ , \tag{13}$$

where the numbers in parentheses correspond to the Hofstadter limits with a mean π^0 multiplicity of 3.

We have also observed states with masses between those of the ψ' and the ψ by observing the hadronic decay modes of these intermediate states[11] as follows:

$$\psi' \to \gamma\chi \ , \quad \chi \to \begin{cases} \pi^+\pi^-\pi^+\pi^- \\ \pi^+\pi^-\pi^+\pi^-\pi^+\pi^- \\ \pi^+\pi^- K^+K^- \\ \pi^+\pi^- \text{ and/or } K^+K^- \end{cases} \tag{14}$$

The one-constraint fitted mass distributions of the hadronic systems of reaction (14) are shown in Fig. 18. The shaded regions show those events consistent with the direct decay of the ψ' into charged particles with no γ-ray (4-constraint fits). The 4-pion mass distribution of Fig. 18a shows two distinct peaks, one at 3.41 GeV with the FWHM of ~20 MeV, consistent with our resolution, and the other at 3.53 GeV, with the FWHM of ~60 MeV, which is considerably broader than our resolution. The peaks in the 6-pion and ππKK mass distributions tend to confirm the 4-pion results. There are insufficient data in these channels to prove independently the existence of two states.

The $\pi\pi$ or KK distribution of Fig. 18d shows only one peak at a mass of 3.41 GeV corresponding to the lower of the two peaks in the 4-pion distribution. Because of this decay mode, this state must have natural spin-parity as well as even charge conjugation, i.e., $J^{PC} = 0^{++}, 2^{++}, \ldots$.

Table VI gives our measurements of the product branching fractions of the intermediate states for decay by a particular mode. Each of these branching fractions is the product of the branching fraction of ψ' decay to that state times the branching fraction of the state to a particular mode.

Recently, the group has improved the mass resolution of the detector by including in the analysis programs more accurate magnetic-field maps, better alignment data, etc. The result is that the broad 3.53-GeV state as seen in the 4π decay mode seems to separate into two states: one at about 3.50 GeV and the other at about 3.55 GeV. This analysis does not yet include the recent data.

We can conclude from the experimental evidence that at least three states exist with a mass between that of the ψ' and the ψ. Two of these states are the narrow states $\chi(3410)$ and $P_c(3500)$ or (3270) with observed widths consistent with our resolution. A third state is the $\chi(3530)$, with an observed width larger than the experimental resolution. It is tempting to suppose that three narrow states exist and that the broad $\chi(3530)$ seen in the charged particle decay modes is actually two unresolved narrow states at $\sim$3500 MeV and 3550 MeV. The recent work on the 4π mode of the (3530) tends to confirm this view. The lower of these states could then be identified with the P_c whose mass would be fixed at 3500. The production branching fraction of both (3500) and (3550) to 4π's would then be about the same, while the $\gamma\psi$ branching fraction of (3500) would be much greater than that of the (3550). This question cannot be settled until the recent data are completely analyzed.

We have not observed the state X reported by the DASP and DESY-Heidelberg collaborations. Our limit on the total branching fraction of ψ to X by γ-emission given earlier is less than 7%. The DASP and DESY-Heidelberg groups report the observation of this state through the decay $\psi \to \gamma + X$, $X \to \gamma + \gamma$. The SPEAR magnetic detector has an extremely low trigger efficiency for a 3γ final state, and so it is not possible for us to study this decay mode.

The DASP group also reported a decay of $X \to p\bar{p}$ with a product branching fraction of $\sim 1.5 \times 10^{-4}$. We have searched for this mode and have not found it. With a product branching fraction of 1.5×10^{-4}, we should have seen 15 events in the detector, with a p and $\bar{p}$ of invariant mass corresponding to the X, and with a missing mass of zero corresponding to the γ-ray from the $\psi \to X$ transition. We have no events in this region, and get a 90% confidence limit of

$$\frac{\Gamma(\psi \to \gamma + X)}{\Gamma(\psi \to \text{all})} \times \frac{\Gamma(X \to p + \bar{p})}{\Gamma(X \to \text{all})} < 4 \times 10^{-5} \quad . \tag{15}$$

Some models would make the ψ' decay to X via the emission of an ω a strong transition. We have looked for this transition by searching for $\pi^+\pi^-$ with an invariant mass equal to the ω mass (1.3% decay mode of the ω) and with the proper momentum to correspond to the $\psi' \to \omega + X$ decay. At the same time we searched for the decays $\psi' \to \omega + \eta'$ and $\psi' \to \omega + \eta$. We have not found any of these transitions, and our limits (90% confidence) are

$$\begin{aligned} \Gamma(\psi' \to \omega + X)/\Gamma(\psi' \to \text{all}) &< 8\% \ , \\ \Gamma(\psi' \to \omega + \eta')/\Gamma(\psi' \to \text{all}) &< 4.3\% \ , \\ \Gamma(\psi' \to \omega + \eta)/\Gamma(\psi' \to \text{all}) &< 2.2\% \ . \end{aligned} \tag{16}$$

Figure 19 is a schematic summary of all the new states. Superficially, this diagram looks very must like the prediction of the Charm-Quark model. There is only one state missing, and there is no room for more states other than this missing one in the model. All of the quantum numbers that have been determined

for these states are consistent with those expected for the bound states of two heavy fermions. There may be some problems for the Charm-Quark model with the high-mass 1^{--} states as far as their widths are concerned, and there will be serious problems if the 4.1 GeV state is split into further substates. The most serious problem with the Charm-Quark model is the lack of success so far of the experiments that are specifically hunting for charmed mesons[16] or baryons. Given the amount of effort now going into this search, such particles should be found within a year, if they exist at all.

VII. μ-e EVENTS

As you have all heard by now, the SLAC/LBL group has found what we call "anomalous μ-e events" in the data we have taken at SPEAR. Our first results have been published,[17] and a more detailed review of these data by M. Perl will be published shortly in the proceedings of the 1975 SLAC Summer Institute on Particle Physics. There are many possibilities for the origin of these events. All of the hypotheses have in common the production of a pair of particles, each with an additive conserved quantum number which is zero for the e^+e^- system. Examples are the production and decay of a pair of new heavy leptons or perhaps of a boson pair with a quantum number such as Charm. Before speculating further on the origin of these events, I shall review the event selection criteria and the methods of data analysis.

We have 86 such events (as of September, 1975), of which about 25% are background. All these events are selected from the sample of data which has only two charged particles visible in the detector with any number of neutrals visible in the detector shower counters, and with any number of charged particles or neutrals escaping out of the ends of the detector. The largest single data sample is that at $E^* = 4.8$ GeV, and I shall use this sample to illustrate the analysis procedure.

The 4.8 GeV data set contains 9500 events with ≥ 3 visible prongs and some 25,000 2-prong events. Of these 2-prong events, about 20,000 are Bhabha scatterings and around 1500 are quantum-electrodynamic μ-pair production. In most Bhabha scattering and μ-pair production, the planes defined by each final state particle and the beam direction are coincident, i.e., the events are coplanar. Radiative corrections can make these events a-coplanar, but the cross section decreases rapidly with increasing coplanarity angle. To eliminate most Bhabha and μ-pair events, we require 2-prong events to have a coplanarity angle $\geq 20^\circ$. This cut leaves about 2500 of the original 25,000 events.

The sample is further reduced by momentum cuts and certain geometric restrictions. A μ-meson must have a minimum momentum of 590 MeV/c to reach the muon chambers. Since we do not want to be at the edge of the range cutoff, we require all μ-candidate prongs to have $p \geq 650$ MeV/c. In addition, at low momentum the shower counters are not very effective in discriminating between electron and hadrons. For simplicity we require the e-candidates also to have $p \geq 650$ MeV/c. We also make certain geometric cuts requiring candidate events to have both tracks within the central 90% of the shower counters and to be aimed toward the efficient area of the muon chambers. All these cuts reduce the sample of 2-prong events to 513.

These events are listed in Table VII. The events are classified there according to total charge, the number of associated photons (shower counters hit other than the two hit by charged particles), and the computer particle classification: e, μ, or hadron (h). The eμ events in Column 1 stand out as having a pattern different from the other types of events. These eμ events can not come from 2-photon processes:

$$e^+e^- \rightarrow e^+e^-\mu^+\mu^- \quad . \tag{17}$$

for this process should yield the same numbers of eμ events with charge-0 and with charge-2.

We now need to evaluate the background expected in the eμ column from various kinds of particle misidentification. We have determined the hadron misidentification probabilities from a study of the multiprong events, and lepton misidentification probabilities from the study of a large number of coplanar Bhabha and μ-pair events. In determining the hadron misidentification probabilities, we assume that all tracks in the ≥ 3 prong events are in fact hadrons. If there are real muons and electrons in this sample (not from ordinary hadron decay), we are overestimating the misidentification probability and compute a larger background than is in fact present. In determining these probabilities we weight the momentum distribution of the hadrons to correspond to the momentum distribution observed in the μe events. The misidentification probabilities are given in Table VIII.

From these misidentification probabilities, we evaluate the number of background μe events expected, and find

1) 0 extra photons, 4.7 ± 1.2 background (24 events seen),
2) 1 extra photon, 5.6 ± 1.5 background (8 events seen),
3) ≥ 2 extra photons, 8.6 ± 2.0 background (8 events seen).

The calculated background agrees with the number of μe events seen with ≥ 1 photon, but is very much smaller than the number of events seen with zero photons. There is clearly an anomalous μe signal.

The background can also be evaluated with less statistical accuracy using only the events of Column 1 of Table VII. This method gives 7.9 ± 3 background events, still leaving the anomalous $e\mu$ signal.

There is one further background check, which is more qualitative than quantitative. In the ψ' decay, we have about 75,000 events involving hadronic decays other than to the ψ. Because of the large cross section of the ψ', these events were obtained in a relatively small integrated luminosity. The number of $e\mu$ events found in this sample is consistent with the background calculated as described above. If there were some subtle background effect in multihadron events, one might expect it to show up in this very large sample of hadronic decays.

Data at all energies are treated as described above for 4.8 GeV. The resulting cross section is shown in Fig. 20. The observed cross section is plotted with no corrections for geometric acceptance or for the kinematic cuts made. These corrections cannot be determined without a knowledge of the origin of the events.

We can examine various angular and momentum correlations and distributions to seek further clues to the origin of these events. The simplest such correlation is the invariant mass of the $e\mu$ system vs the missing mass recoiling against the system. This is shown for the 4.8 GeV data in Fig. 21. We can see a broad spread in the $e\mu$ mass and in the missing mass which tells us only that the $e\mu$ combination does not come from the decay of what would be a very peculiar boson and that at least two particles escape detection.

Figure 22 shows the distribution of collinearity angles between the e's and μ's for three center-of-mass energy regions. The curves represent the expected distributions including the effects of our cuts, for the reaction

$$e^+ + e^- \rightarrow U^+ + U^- \quad , \qquad (18)$$

$$U \rightarrow e + X; \quad \text{or} \quad \mu + X \quad ,$$

where X represents one or more neutral particles. For example, if U were a heavy lepton, X might be two neutrinos; while if U were a boson, X might be one neutrino or a neutrino plus K_L^o. The solid curve in Fig. 22 represents the expected distribution for the 3-body decay of a 1.8 GeV mass heavy lepton via a V-A interaction. The spins of the lepton pair are assumed to be uncorrelated. The dotted curve represents the 2-body decay of a 1.9 GeV mass boson. No sharp conclusion can be drawn from this figure: at best there is a mild preference for the 3-body decay.

Figure 23 shows the momenta of all of the e's and μ's vs the center-of-mass energy at which the events were found. The curves on the graph indicate the maximum possible momentum for a lepton coming from a U particle decay, assuming that the neutral masses are zero. The data between 3.8 and 4 GeV might seem to rule out U masses above 1.8 GeV, but this is not the case. A glance at the cross section graph (Fig. 20) shows that the data in this energy interval are only one standard deviation above the feedthrough background, and these events could easily be a background fluctuation. Since all of the background events are included in Fig. 23, we can say with reasonable certainty only that the U mass should be less than ~2.1 GeV.

We can look in more detail at the distributions in momentum. To do this we need a way to combine runs taken at different center-of-mass energies and therefore we define a parameter

$$\rho = \frac{p - 0.65}{p_{max} - 0.65} \tag{19}$$

where p is the momentum of the lepton in GeV/c and p_{max} is the maximum possible momentum a lepton can have from a U-particle decay. Figure 24 shows the distribution of the leptons vs ρ for three energy bands. The parameter p_{max} is that for a 1.8 GeV mass particle. The solid and dotted curves are calculated for a 3-body V-A decay and for a 2-body decay, respectively. The data mildly favors a 3-body decay, but even this conclusion is somewhat sensitive to the choice of U mass: using 2.1 GeV rather than 1.8 GeV makes the choice of the 3-body decay over the 2-body decay less compelling.

The energy dependence of the observed cross section also does not help to distinguish between different types of U particles. The data can be fit equally well with the 1/S dependence expected for a heavy lepton, the $1/S^3$ dependence that might be expected for a pseudoscalar boson, or the $1/S^2$ dependence that might be expected for a vector boson.

We have begun systematically to go through the data searching for μe events with other charged particles or photons associated with the muon and electron tracks. The presence or absence of such events can tell us about the origin of the μe events already discussed. For example, if we hypothesize we are observing the reaction

$$e^+ + e^- \rightarrow U^+ + U^- , \tag{20}$$

and that a U is a heavy lepton, the μe events will arise from the purely leptonic decays

$$U^+ \rightarrow \ell^+ \nu_\ell \bar{\nu}_U , \tag{21a}$$

$$U^- \rightarrow \ell^- \bar{\nu}_\ell \nu_U . \tag{21b}$$

Semileptonic decays are of the form

$$U \rightarrow \nu_U + \text{hadrons} . \tag{22}$$

Since semileptonic decays have no muon or electron in the final state, we should not find μe events in association with extra charged particles or photons.

The situation is quite different if U is a hadron (a charmed particle, for example). In that case, we can have purely leptonic decays, such as

$$U^\pm \rightarrow \ell^\pm + \nu ; \tag{23}$$

semileptonic decays, such as

$$U^\pm \rightarrow \ell^\pm + \nu + \text{hadrons} ; \tag{24}$$

and non-leptonic decays, such as

$$U^\pm \rightarrow \text{hadrons} . \tag{25}$$

Reaction (24) gives μe events with other particles. In addition, if U is a hadron, we also expect

$$e^+ + e^- \rightarrow U^+ + U^- + \text{hadrons} \tag{26}$$

to be as large as/or larger than reaction (20) when we are a reasonable distance above threshold.

Table IX shows what the computer calls μe events classified according to the total number of charged particles (including the μ and e) and the number of extra γ-rays. In each box the number of events seen is indicated in the upper left while the expected background is indicated in the lower right. (The number of μe events with no extra particles or γ-rays is slightly different from the number in the analysis of the cross section for the cuts made here are slightly different.) There is no significant excess above background except for the μe events without extra associated particles. Summing all the entries in the charge-0 section of the table except the 2-prong no-γ, and subtracting the background, we find

$$\mu e + \text{something} \equiv N(\mu e+) = 37 \pm 21 , \tag{27}$$

as compared to the number with no extra particles,

$$\mu e + \text{nothing} \equiv N(\mu e) = 49 \pm 8 . \tag{28}$$

These numbers are consistent with heavy lepton production and decay. The cross section for reaction (26) is expected to be zero in this case, while the cross section for (20) is expected to be equal to the μ-pair production cross section a few hundred MeV above threshold. If the U is a heavy lepton, we can estimate the leptonic branching fraction to be about 17% each to (e + neutrinos) and (μ + neutrinos).

It is more difficult to say whether (27) and (28) are consistent with a boson decay, for to do so we must make some assumptions about the relative rates for (20) and (26), and about the relative strengths of the pure leptonic and semileptonic decay modes. We shall first assume that all the μe events come from the decay of a pair of mesons with very small pure-leptonic decay modes (such as the charmed D or F), so that all the μe events with no extra particles come from the semileptonic decays

where the other particles escape the detector. We can then compute the expected ratio $N(\mu e)/N(\mu e+)$. To do this we need to specify the semileptonic decay modes and the ratio of cross sections for (20) and (26). We can get an upper bound by assuming that the cross section for reaction (26) is zero, and that all semileptonic decays are

$$U^{\pm} \rightarrow \ell^{\pm} + \nu + K^0 , \qquad (29)$$

for this decay mode gives the largest probability of missing the extra particles of all possible semileptonic decays. The K^0 decays 50% of the time to K_L^0 which will not be seen in the detector, and 50% of the time to K_S^0. All the K_S^0 decay products will be missed about 10% of the time. In this case, $N(\mu e)/N(\mu e+)$ should be $\geq 1/2$. Given $N(\mu e) = 49 \pm 8.5$, we expect $N(\mu e+) \geq 98 \pm 17$, while we observed 37 ± 21. We conclude that particles like the charmed D or F with very small pure-leptonic branching fractions are not likely to be the source of the μe events.

If we hypothesize a hadron with roughly equal leptonic and semileptonic decay modes (the D* and F*, for example), the situation is more complicated. The relative detection efficiencies for the leptons from the pure-leptonic and semileptonic decay modes will depend on the dynamics of the semileptonic decay. To get some idea of what we might expect, we shall ignore this difference and further assume that the cross section for (26) equals the cross section for (20). This probably underestimates the cross section for (26) except near threshold. If we make the same analysis as above, ie., assuming all semileptonic decays are $\ell \nu K^0$, we find again $N(\mu e)/N(\mu e+) \approx 1/2$. Thus, charmed particles like the D* and F* can probably also be ruled out as the origin of the μe events, although this conclusion is not as strong as in the previous paragraph because of the problem of detection efficiencies.

Finally, there is one bit of evidence that comes from the Maryland-Pavia-Princeton group (MPP) which also worked at SPEAR.[18] This group used a single-arm spectrometer with a muon identifier and had in addition a nearly-4π system of tracking chambers surrounding the SPEAR interaction region. They looked for muons in association with other charged tracks. There are two classes of events: those with a particle in the spectrometer and ≥ 2 extra prongs in the tracking chambers, and those with a particle in the spectrometer and only one extra prong. The minimum momentum in the spectrometer was 1.05 GeV/c. In the class with ≥ 2 extra prongs, they have 73 events, and 2 of them give a muon signature. They expect 5 background events from pion decay and punch-through. There is therefore no signal in this class. In the class of events with only one extra charged particle, there are 13 events, all of which have a muon in the spectrometer. (The coplanarity and colinearity cuts are described in their paper.) The background is estimated to be 3 events from radiative μ-pair production, and one from hadron decay and punch-through. There does seem to be a signal in this class. The MPP results also hint that the source of the muons is more likely to be a heavy lepton decay than a hadron decay, for the mean charged-particle multiplicity for lepton decay is about 1-1.5 while that for hadron decay is about 2- 2.5.

I can summarize the situation as follows:

(1) Events with a muon and an electron and no extra charged particles exist. Only about 25% of the events can be explained as background.

(2) The momentum spectrum of the leptons and their colinearity angle distribution both favor a 3-body decay as the source of the μe events, although neither a 2-body decay nor a mixture of 2- and 3-body decays is completely excluded.

(3) The threshold for the μe events lies between 3.8 and 4 GeV c.m., implying that the mass of the parent particle is 1.9- 2 GeV.

(4) The energy dependence of the observed μe cross section mildly favors 1/S.

(5) The search for μe events with associated γ-rays or hadrons appears to exclude the 3-body semileptonic decay of a hadron as a source of the μe events. This implies that pseudoscalar / charmed-particle production and decay have nothing to do with the μe events. The states involved cannot be D or F.

(6) The same type of analysis as in (5) indicates that the D* and F* are also unlikely sources for the μe events. More work needs to be done on detection efficiency calculations before this point can be made more sharply.

(7) MPP multiplicity data indicate a low charged-particle multiplicity associated with their observed muons.

(8) All data are consistent with the hypothesis that the μe events come from the decay of the pair of heavy leptons. While hadron production and decay are not completely ruled out, it becomes increasingly unlikely as the analysis proceeds.

(9) If the U is a heavy lepton, the branching fraction is 17% each to $e\nu\nu$ and $\mu\nu\nu$.

What is needed now is more data taken with different kinds of apparatus with different types of biases. We expect roughly to double the data we have now with the SLAC/LBL magnetic detector in the next six months. In addition, two new experiments will be run at SPEAR in the coming year. One of these will look at the μ-inclusive spectrum (not requiring two leptons), while the other will look at the e-inclusive spectrum. The MPP group is back at SPEAR and is now taking more data, and the DASP and PLUTO spectrometers at DESY have begun to study these anomalous lepton events. Hopefully, we can understand the origin of these phenomena during the coming year.

REFERENCES

1. J. E. Augustin et al., Phys. Rev. Letters 33, 1406 (1974); G. S. Abrams et al., Phys. Rev. Letters 33, 1453 (1974).
2. J. J. Aubert et al., Phys. Rev. Letters 33, 1404 (1974).
3. For a description of the ring, see SPEAR Storage Ring Group, Proceedings of IX International Conference on High Energy Accelerators, Stanford, California, 1974, p. 37.
4. Members of the SLAC/LBL collaboration: G. S. Abrams. J. E. Augustin, A. M. Boyarski, M. Breidenbach, D. Briggs, F. Bulos, W. Chinowsky, G. J. Feldman, G. E. Fischer, C. E. Friedberg, D. Fryberger, G. Goldhaber, G. Hanson, D. L. Hartill, R. J. Hollebeek, B. Jean-Marie, J. A. Kadyk, R. R. Larsen, A. M. Litke, D. Luke, B. A. Lulu, V. Luth, H. L. Lynch, D. Lyon, C. C. Morehouse, J. M. Paterson, M. L. Perl, F. M. Pierre, T. P. Pun, P. Rapidis, B. Richter, B. Sadoulet, R. F. Schwitters, W. Tanenbaum, G. H. Trilling, F. Vannucci, J. S. Whitaker, F. C. Winkelmann, J. E. Wiss, and J. E. Zipse.
5. A. M. Boyarski et al., Phys. Rev. Letters 34, 1357 (1975).
6. V. Luth et al., Phys. Rev. Letters 35, 1124 (1975).
7. B. Jean-Marie et al., Phys. Rev. Letters 36, 289 (1976).
8. A. M. Boyarski et al., Phys. Rev. Letters 34, 762 (1975).
9. D. C. Hom et al., submitted to Phys. Rev. Letters.
10. Part of this data has been published: J. E. Augustin et al., Phys. Rev. Letters 34, 764 (1975).
11. G. J. Feldman et al., Phys. Rev. Letters 35, 821 (1975).
12. W. Tanenbaum et al., Phys. Rev. Letters 35, 1323 (1975).
13. W. Braunschweig et al., Phys. Letters 57B, 407 (1975).
14. B. Wiik, Proceedings of the International Conference on Lepton-Photon Interactions, Stanford University, August 1975.
15. J. W. Simpson et al., Phys. Rev. Letters 35, 699 (1975).
16. A. M. Boyarski et al., Phys. Rev. Letters 35, 196 (1975).
17. M. L. Perl et al., Phys. Rev. Letters 35, 1489 (1975).
18. M. Cavalli-Sforza et al., Phys. Rev. Letters 36, 558 (1976).

TABLE I

Properties of the ψ-particles as obtained from fit to cross sections σ_{Had}, $\sigma_{\mu\mu}$ and σ_{ee}. Errors accounted for: (a) statistical, (b) 15% uncertainty on hadron efficiency, (c) 100-keV setting error in E*, (d) 2% point-to-point errors, uncorrelated, (e) 3% luminosity normalization.

Property	$\psi(3095)$	$\psi(3684)$
Mass	3.095 ± 0.004 GeV	3.684 ± 0.005 GeV
J^{PC}	1^{--}	1^{--}
$\Gamma_e = \Gamma_\mu$	4.8 ± 0.6 keV	2.2 ± 0.3 keV
Γ_H	59 ± 14 keV	220 ± 56 keV
Γ	69 ± 15 keV	225 ± 56 keV
Γ_e/Γ	0.069 ± 0.009	0.0097 ± 0.0016
Γ_H/Γ	0.86 ± 0.02	0.981 ± 0.003
Γ_μ/Γ_e	1.00 ± 0.05	0.89 ± 0.16

TABLE II

Decay modes of the $\psi(3095)$

Mode	Branching ratio (%)	Number of events Observed	Comments
e^+e^-	6.9 ± 0.9	~ 2000	.....
$\mu^+\mu^-$	6.9 ± 0.9	~ 2000	.....
$\rho\pi$	1.3 ± 0.3	153 ± 13	$> 70\%$ of $\pi^+\pi^-\pi^0$
$2\pi^+ 2\pi^-$	0.4 ± 0.1	76 ± 9	.....
$2\pi^+ 2\pi^- \pi^0$	4.0 ± 1.0	675 ± 40	$\begin{cases} 20\% & \omega\,\pi^+\pi^- \\ 30\% & \rho\,\pi\pi\pi \end{cases}$
$3\pi^+ 3\pi^-$	0.4 ± 0.2	32 ± 7	.....
$3\pi^+ 3\pi^- \pi^0$	2.9 ± 0.7	181 ± 26	.....
$4\pi^+ 4\pi^- \pi^0$	0.9 ± 0.3	13 ± 4	.....
$\pi^+\pi^- K^+K^-$	0.4 ± 0.2	83 ± 18	not including $K^*(892)$ $K^*(1420)$
$2\pi^+ 2\pi^- K^+K^-$	0.3 ± 0.1	.....	.....
$K_S K_L$	< 0.02	≤ 1	90% confidence limit
$K^0 K^{0*}(892)$	0.24 ± 0.05	57 ± 12	.....
$K^\pm K^{\mp *}(892)$	0.31 ± 0.07	87 ± 19	.....
$K^0 K^{0*}(1420)$	< 0.19	≤ 3	90% confidence limit
$K^\pm K^{\mp *}(1420)$	< 0.19	≤ 3	90% confidence limit
$K^{0*}(892)\ \bar{K}^{0*}(892)$	< 0.06	≤ 3	90% confidence limit
$K^{0*}(1420)\ \bar{K}^{0*}(1420)$	< 0.18	≤ 3	90% confidence limit
$K^{0*}(892)\ K^{0*}(1420)$	0.37 ± 0.10	30 ± 7	.....
$p\bar{p}$	0.23 ± 0.013	331 ± 18	assuming $f(\theta) \approx 1 + \cos^2\theta$
$\Lambda\bar{\Lambda}$	0.16 ± 0.08	19 ± 5	.....
$p\ \bar{p}\ \eta$	0.06 ± 0.015	82 ± 20	preliminary
$p\ \bar{p}\ \pi^0$ $n\ p\ \pi^-$ $\bar{p}\ n\ \pi^+$	0.37 ± 0.19	87 ± 30	.....

TABLE III

Decay Modes of the $\psi(3684)$

Modes	Branching Ratio (%)	Comments
e^+e^-	0.97 ± 0.16	} μe universality assumed
$\mu^+\mu^-$	0.97 ± 0.16	
$\psi(3100)$ anything	57 ± 8	.....
$\psi(3100)\ \pi^+\pi^-$	32 ± 4	} these decays are included in the fraction for ψ + anything
$\psi(3100)\ \eta^0$	4 ± 2	
$\rho^0\pi^0$	< 0.1 *	.....
$2\pi^+\ 2\pi^-\pi^0$	0.35 ± 0.15	.....
$p\bar{p}$	0.04 ± 0.02	.....
$\pi^+\pi^-K^+K^-$	~ 0.05	.....
$\chi(3410)\ \gamma$	7 ± 3	assumes isotropic γ angular distribution

* 90% confidence limit based on a preliminary analysis

Table IV

Results of the search for narrow resonances. Upper limits (90% confidence level) for the radiatively corrected integrated cross section of a possible narrow resonance. The width of this resonance is assumed to be small compared to the mass resolution.

Mass Range (GeV)	Limit on $\int \sigma_H \, dE_{c.m.}$ (nb MeV)
3.20 → 3.50	970
3.50 → 3.69	780
3.72 → 4.00	850
4.00 → 4.40	620
4.40 → 4.90	580
4.90 → 5.40	780
5.40 → 5.90	800
5.90 → 7.60	450

Table V

Summary of the masses, widths, areas, and couplings to the e^+e^- systems.

Mass (GeV)	Γ_{tot} (MeV)	$\int \sigma \, dE^*$ (nb-GeV)	$\Gamma_{e^+e^-}$ (keV)
3.1	0.069	10.4	4.8
3.7	0.225	3.7	2.2
3.95	60.	0.35	0.2
4.1	200	2.5	1.8
4.4	40	0.25	0.2

Table VI

Product branching fractions in % for various decay modes of the intermediate states χ and P_C.

Decay mode	$\chi(3410)$	$\chi(3530)$	P_C
$4\pi^{\pm}$	0.14 ± 0.07	0.2 ± 0.1	?
$6\pi^{\pm}$	~ 0.1	~ 0.2	?
$\pi^+\pi^-K^+K^-$	~ 0.07	~ 0.05	?
$\pi^+\pi^-$ or K^+K^-	0.13 ± 0.05	< 0.027	< 0.027
$\gamma\psi$	< 0.5	?	3.6 ± 0.7

Table VII

2-prong events at $E_{cm} = 4.8$. p_1 and $p_2 \geq .65$ GeV, $\theta_{coplanar} \geq 20^o$.

	Total Charge 0 Extra Shower Counter			Total Charge 2 Extra Shower Counter		
	0	1	≥ 2	0	1	≥ 2
ee	40	111	55	0	1	0
$e\mu$	24	8	8	0	0	3
$\mu\mu$	16	15	6	0	0	0
eh	20	21	32	2	3	3
μh	17	14	31	4	0	5
hh	14	10	30	10	4	6

Table VIII

Particle misidentification probabilities.

p (h → e)	0.18 ± 0.01
p (h → μ)	0.20 ± 0.01
p (e → h)	0.056 ± 0.010
p (e → μ)	0.011 ± 0.002
p (μ → h)	0.08 ± 0.01
p (μ → e)	< 0.01

TABLE IX

All μe events classified according to the total number of visible tracks, the number of photons detected, and the charge of the μe system. In each box, the number at the upper left is the events found, while that at the lower right is the expected background.

Number of tracks	$\Delta Q = 0$		$\Delta Q = 2$	
	0 γ	$\geq 1\ \gamma$	0 γ	$\geq 1\ \gamma$
2	62 / 13	33 / 33	4 / 3	4 / 4
3	26 / 27	86 / 74	10 / 12	44 / 39
4	29 / 30	137 / 124	18 / 17	95 / 75
≥ 5	17 / 13	119 / 109	12 / 10	81 / 76

FIGURE CAPTIONS

1. Exploded view of the magnetic detector.
2. Schematic end-view of the magnetic detector.
3. Total cross section for e^+e^- to hadrons.
4. Ratio of the μ-pair cross section to the Bhabha cross section in the region of the ψ (a) and ψ' (b) resonances. The solid curves are the expected shapes for 1^{--} resonances interfering with the QED μ-pair production. The dashed curves are for no interference.
5. The front/back asymmetry in μ-pair production in the region of the ψ (a) and ψ' (b) resonances.
6. The ratio of the ratios of hadron to μ-pair production on and off the ψ resonance for various numbers of pions in the final state.
7. Fine scan of total cross section from c.m. energy of 3.2 to 7.7 GeV.
8. Total hadronic cross section vs c.m. energy, including results to September 1975. The radiative tails of the ψ resonances have been subtracted.
9. R vs c.m. energy, with the data of Fig. 5.
10. R on an expanded scale covering the 3-5 GeV region. The open circles are from Ref. 6, and the solid circles include data up to the time of the Photon Conference.
11. A further expansion of the energy scale for R, including the most recent data of October and November 1975.
12. The photon detection efficiency in the pair spectrometer made assuming an isotropic photon angular distribution and $|\cos\theta| \leq 0.6$.
13. Inclusive γ spectrum (a) from ψ' decay, and (b) from ψ decay.
14. Dimuon mass distribution for c.m. energy equal to the ψ' mass. The upper peak is the direct ψ' decay to two muons plus the QED μ-pair production, while the lower peak is from the cascade decay $\psi' \to \psi$ with the ψ decaying into two muons.
15. The $\gamma\psi$ mass distribution as observed in the decay $\psi' \to \psi\gamma\gamma$. The curves are explained in the text.
16. Scatter plot of the two solutions for the mass of intermediate states in $\psi' \to \psi\gamma e^+e^-$.
17. (Missing mass)^2 recoiling against the ψ before and after subtraction of $\psi' \to \psi\pi\pi$.

18. Invariant hadron mass distributions for the constrained fit of $\psi' \rightarrow \gamma$ + hadrons. The hadron systems are (a) 4π, (b) 6π, (c) $\pi\pi KK$, (d) the sum of $\pi^+\pi^-$ and K^+K^-.
19. Energy level diagram of the new states.
20. The observed cross section for the μe events.
21. Distribution of the μe (invariant mass)^2 vs (missing mass)^2 for the data at $E^* = 4.8$ GeV.
22. Distribution of cos θ_{col} for three different c.m. energy intervals. The curves are explained in the text.
23. Distribution of p_e and p_μ for all $e\mu$ events. The curves are upper limits on p_e or p_μ for the indicated U masses in GeV/c^2. These limits are the same for 2-body and 3-body decay provided all neutral masses are zero.
24. The distribution in ρ for three intervals of c.m. energy. The solid and dotted curves are explained in the text.

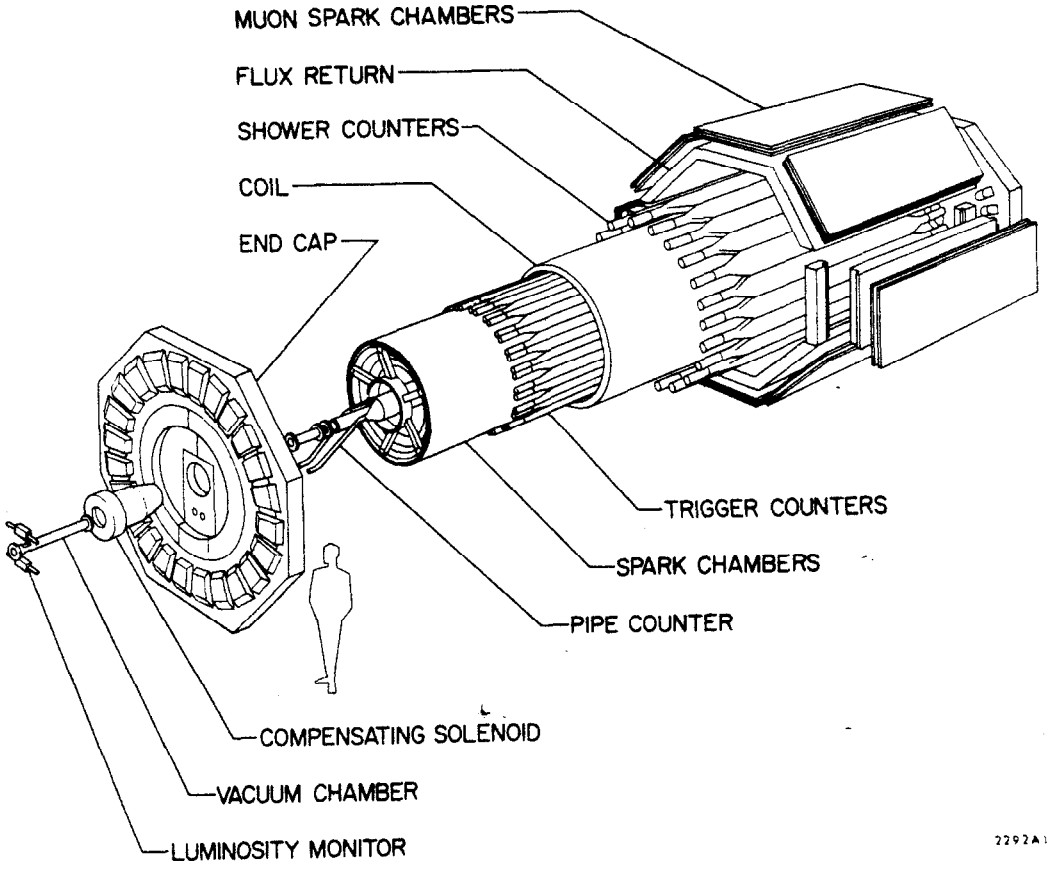
MUON SPARK CHAMBERS
FLUX RETURN
SHOWER COUNTERS
COIL
END CAP
TRIGGER COUNTERS
SPARK CHAMBERS
PIPE COUNTER
COMPENSATING SOLENOID
VACUUM CHAMBER
LUMINOSITY MONITOR
2292A1

Fig. 1

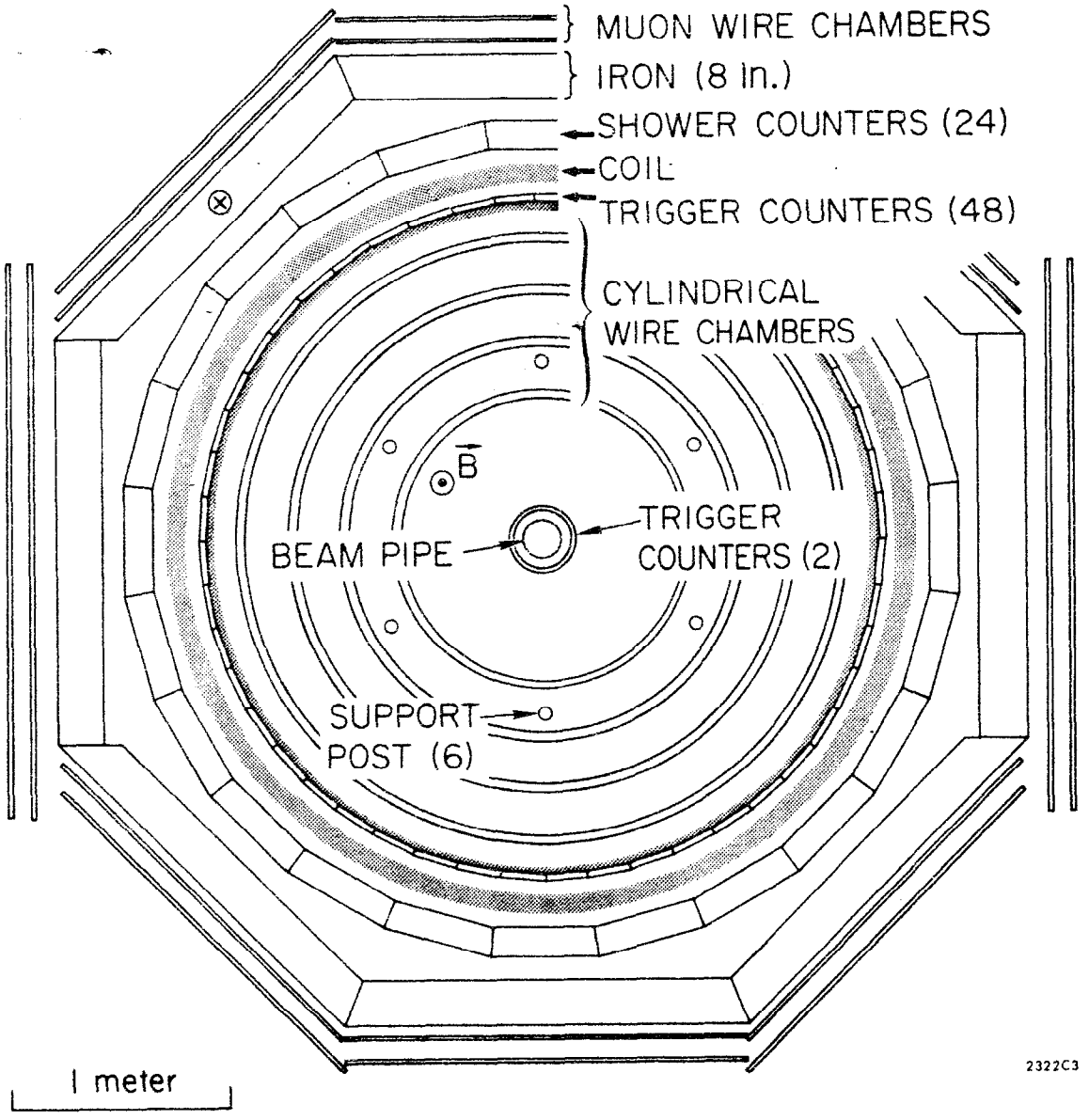
MUON WIRE CHAMBERS
IRON (8 in.)
SHOWER COUNTERS (24)
COIL
TRIGGER COUNTERS (48)
CYLINDRICAL
WIRE CHAMBERS
B
BEAM PIPE
TRIGGER
COUNTERS (2)
SUPPORT
POST (6)
1 meter
2322C3

Fig. 2

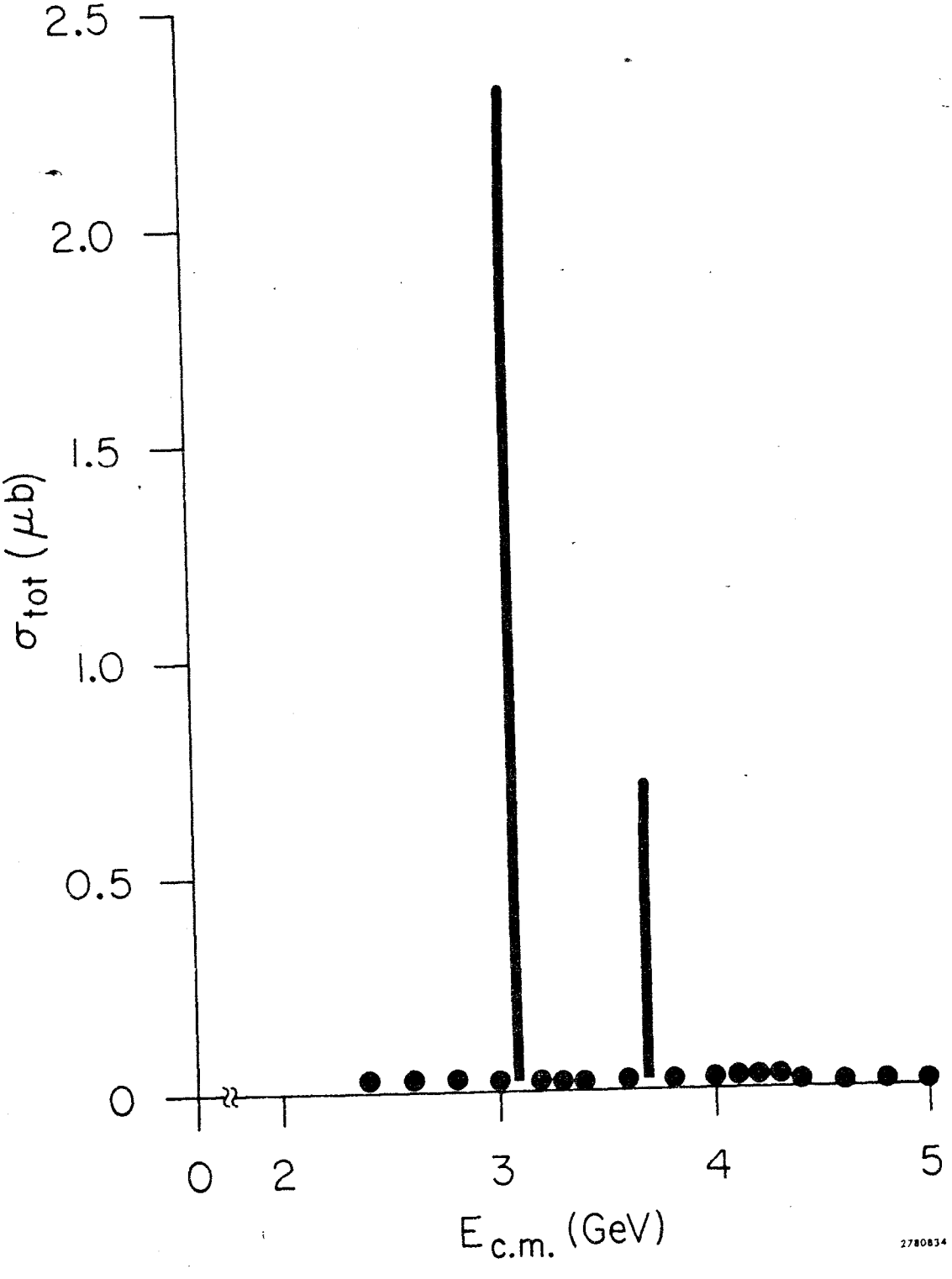

Fig. 3

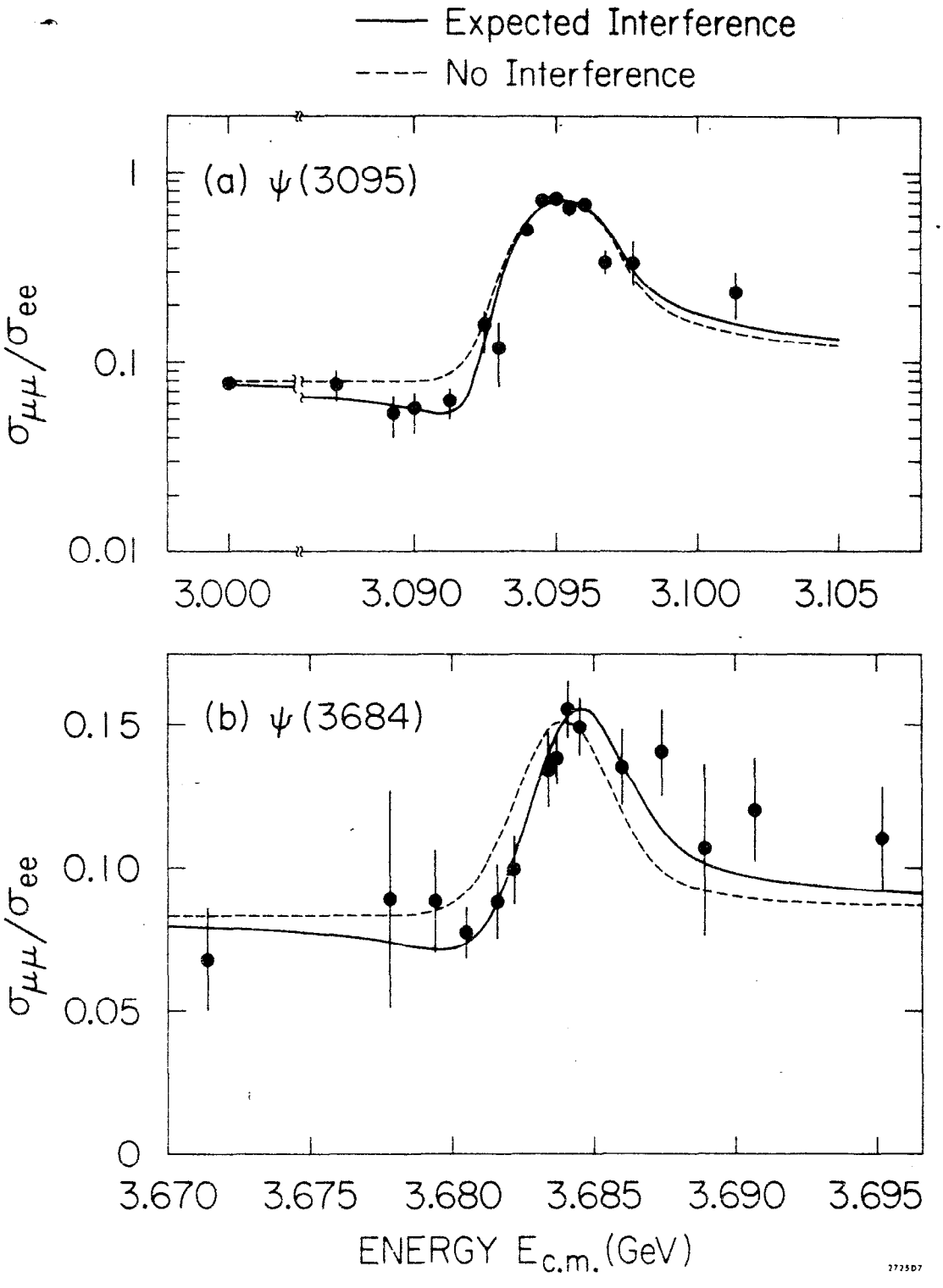
Expected Interference
No Interference
(a) ψ(3095)
(b) ψ(3684)
$\sigma_{\mu\mu}/\sigma_{ee}$
1
0.1
0.01
0.15
0.10
0.05
0
3.000
3.090
3.095
3.100
3.105
3.670
3.675
3.680
3.685
3.690
3.695
ENERGY $E_{c.m.}$ (GeV)
2725D7

Fig. 4

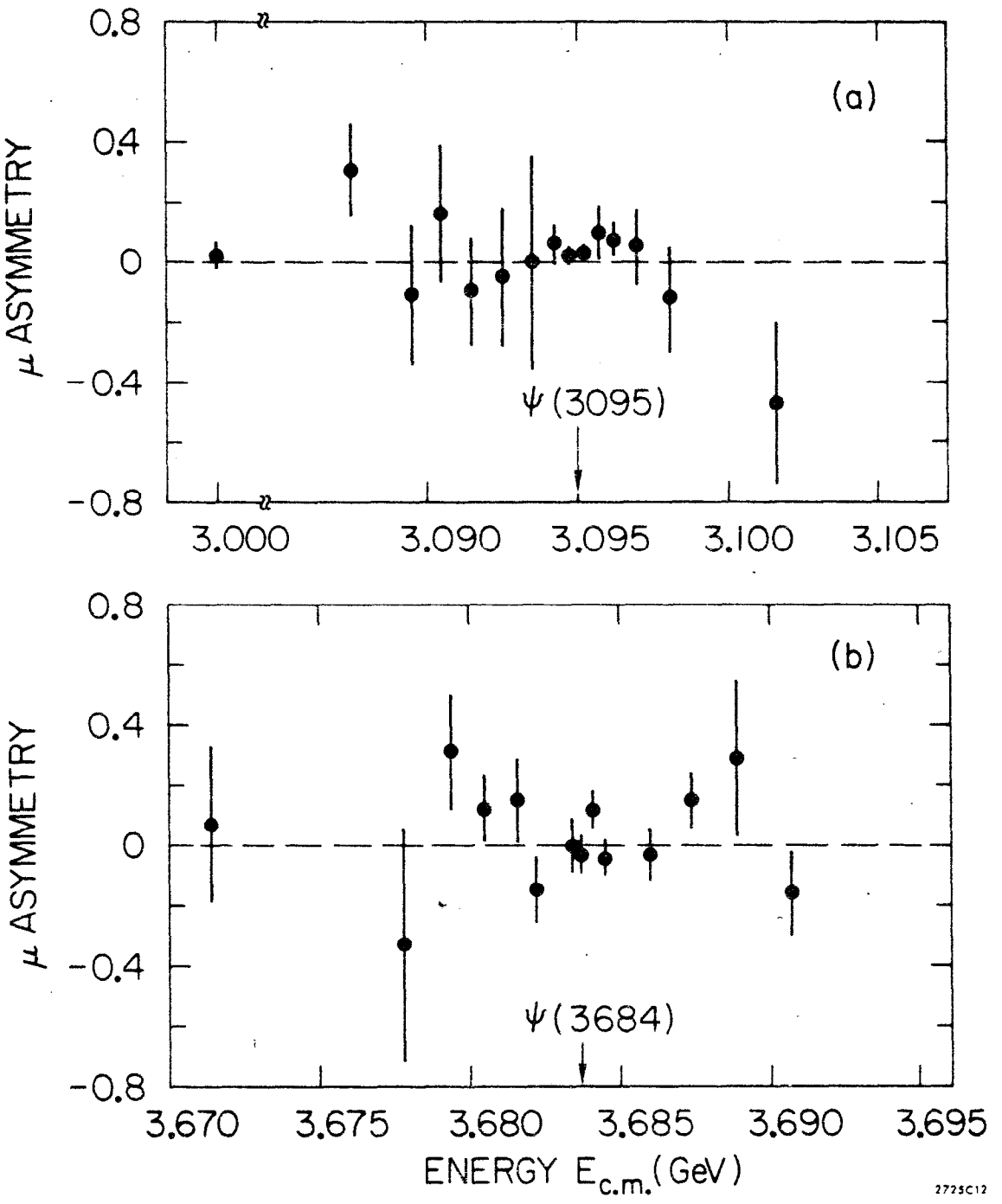
0.8
0.4
0
-0.4
-0.8
μ ASYMMETRY
(a)
ψ(3095)
3.000
3.090
3.095
3.100
3.105
0.8
0.4
0
-0.4
-0.8
μ ASYMMETRY
(b)
ψ(3684)
3.670
3.675
3.680
3.685
3.690
3.695
ENERGY E c.m. (GeV)
2725C12

Fig. 5

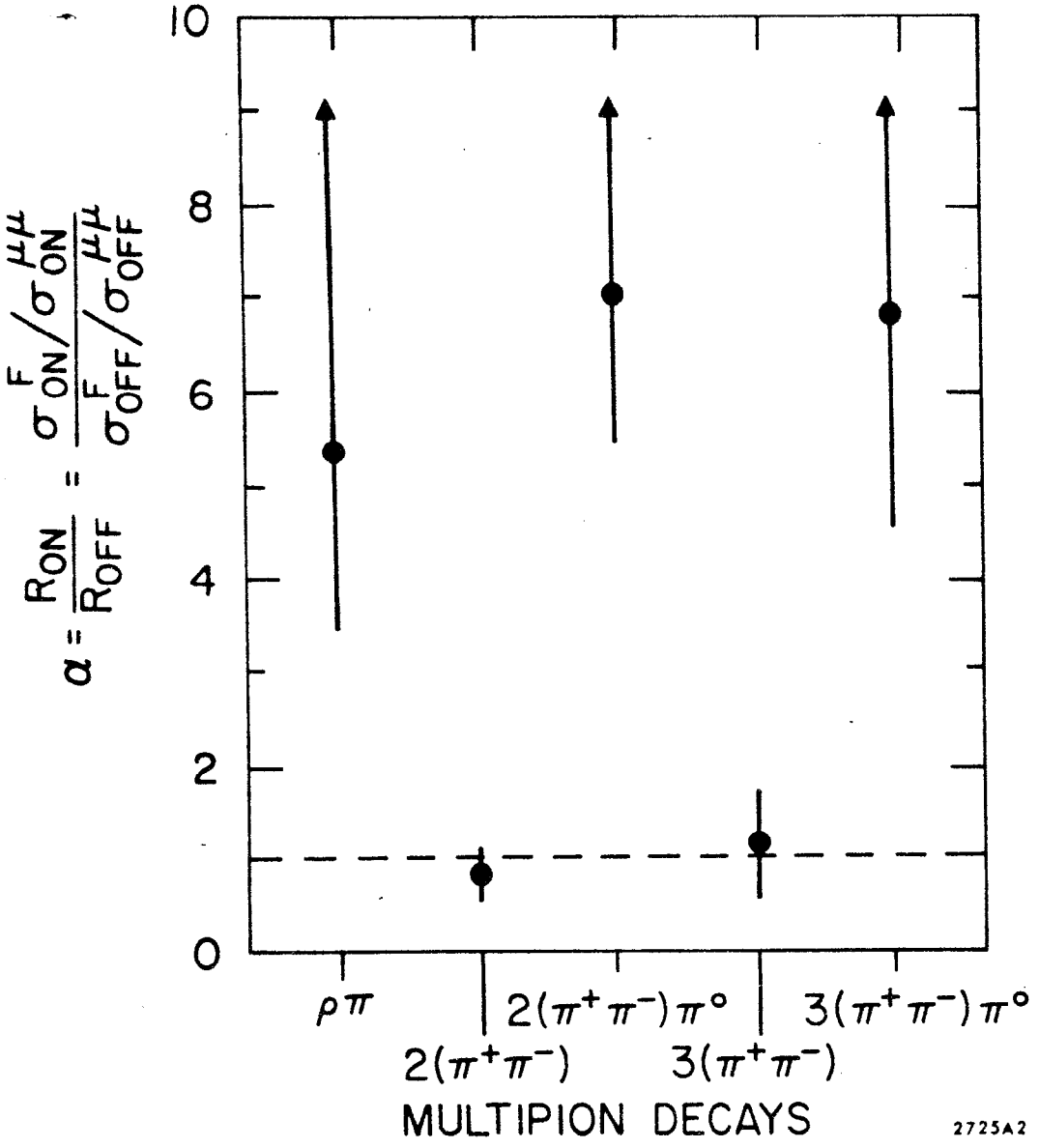
$\alpha = \frac{R_{ON}}{R_{OFF}} = \frac{\sigma^{F}_{ON}/\sigma^{\mu\mu}_{ON}}{\sigma^{F}_{OFF}/\sigma^{\mu\mu}_{OFF}}$
10
8
6
4
2
0
$\rho\pi$
$2(\pi^+\pi^-)\pi^\circ$
$3(\pi^+\pi^-)\pi^\circ$
$2(\pi^+\pi^-)$
$3(\pi^+\pi^-)$
MULTIPION DECAYS
2725A2

Fig. 6

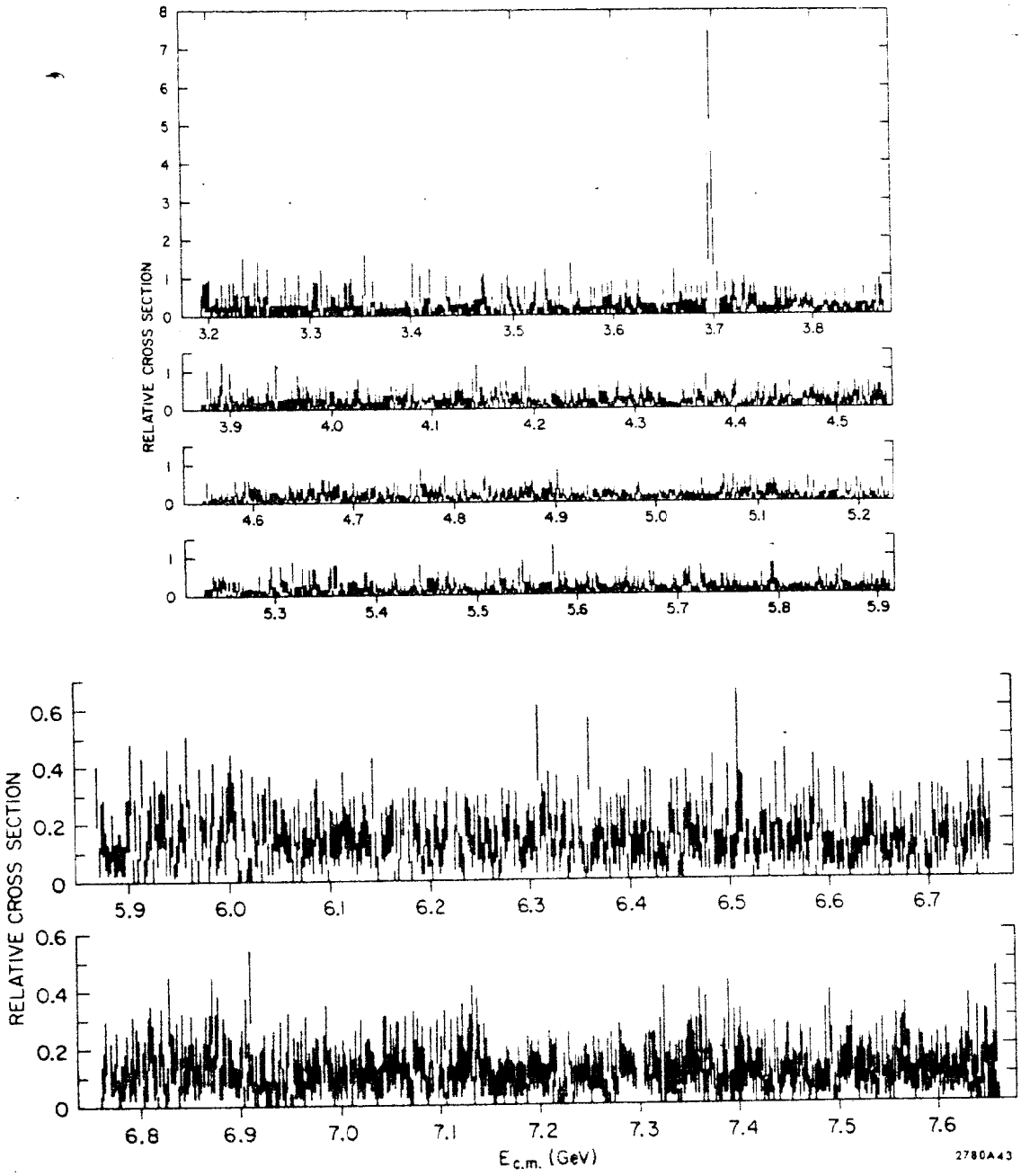

Fig. 7

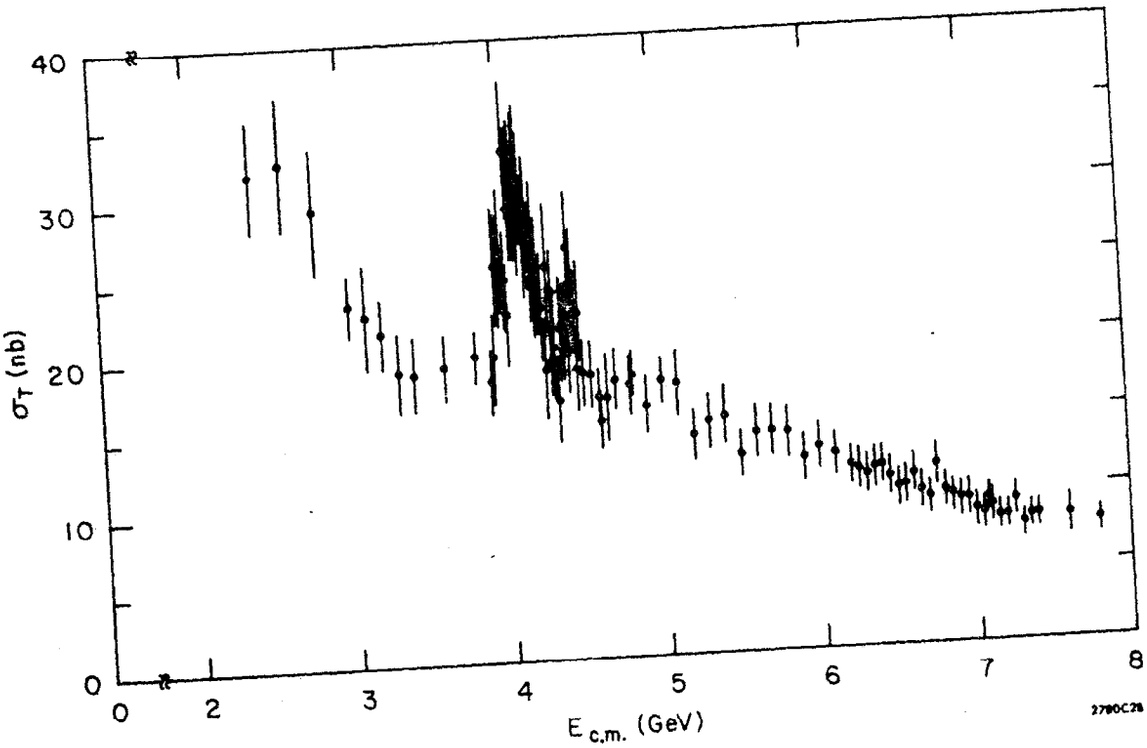

Fig. 8

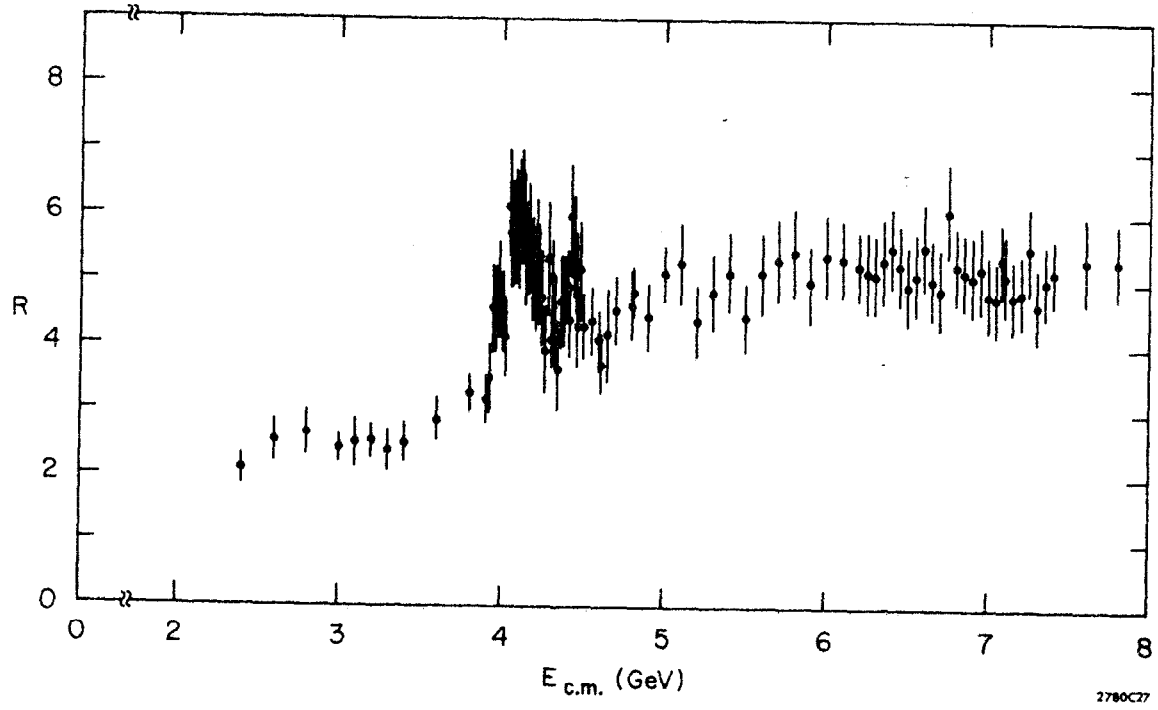

Fig. 9

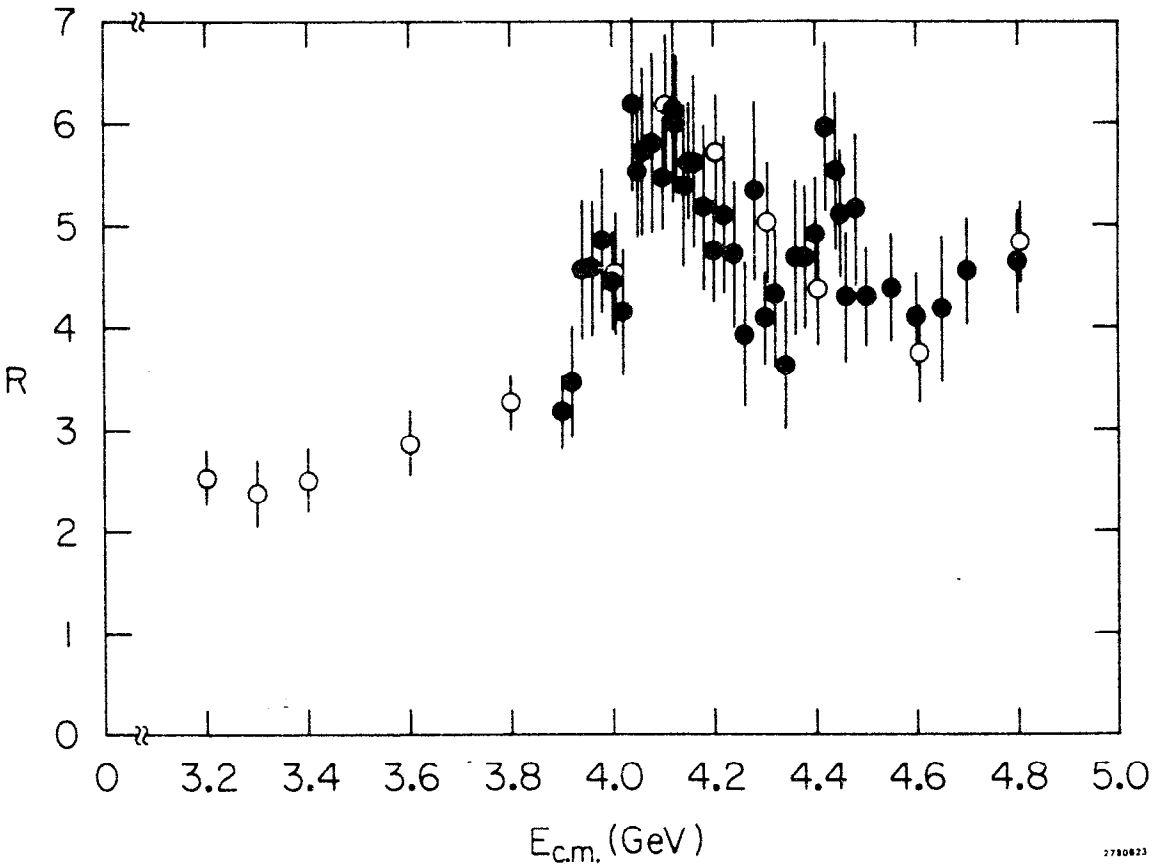

Fig. 10

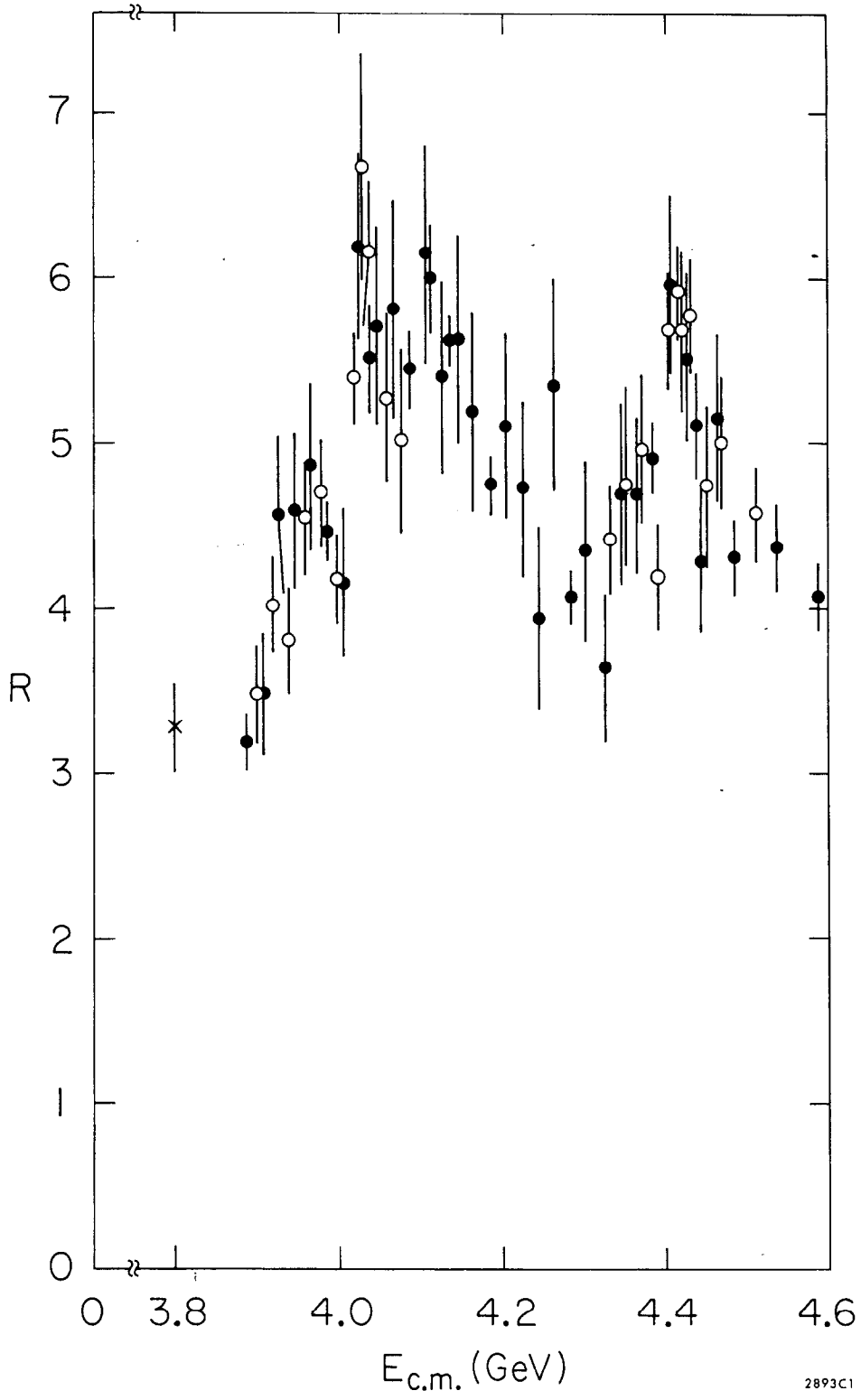

Fig. 11

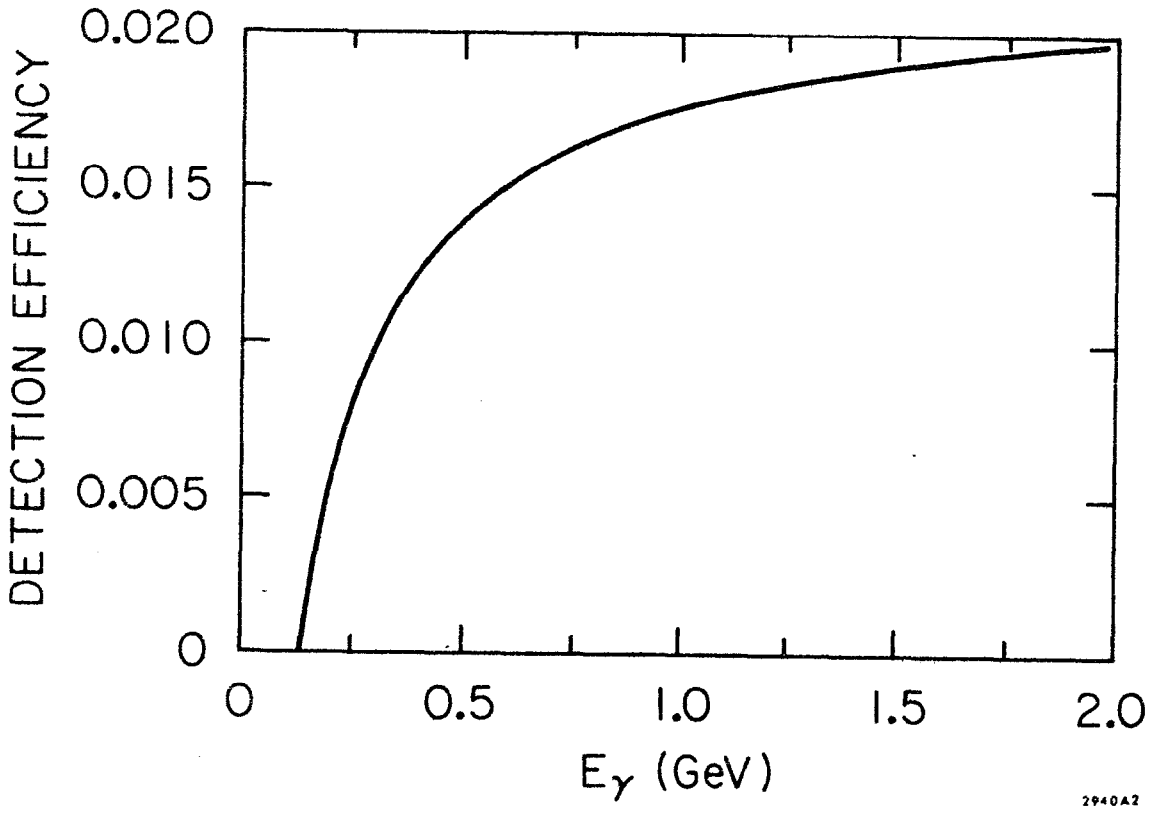
DETECTION EFFICIENCY
0.020
0.015
0.010
0.005
0
0
0.5
1.0
1.5
2.0
E_γ (GeV)
2940A2

Fig. 12

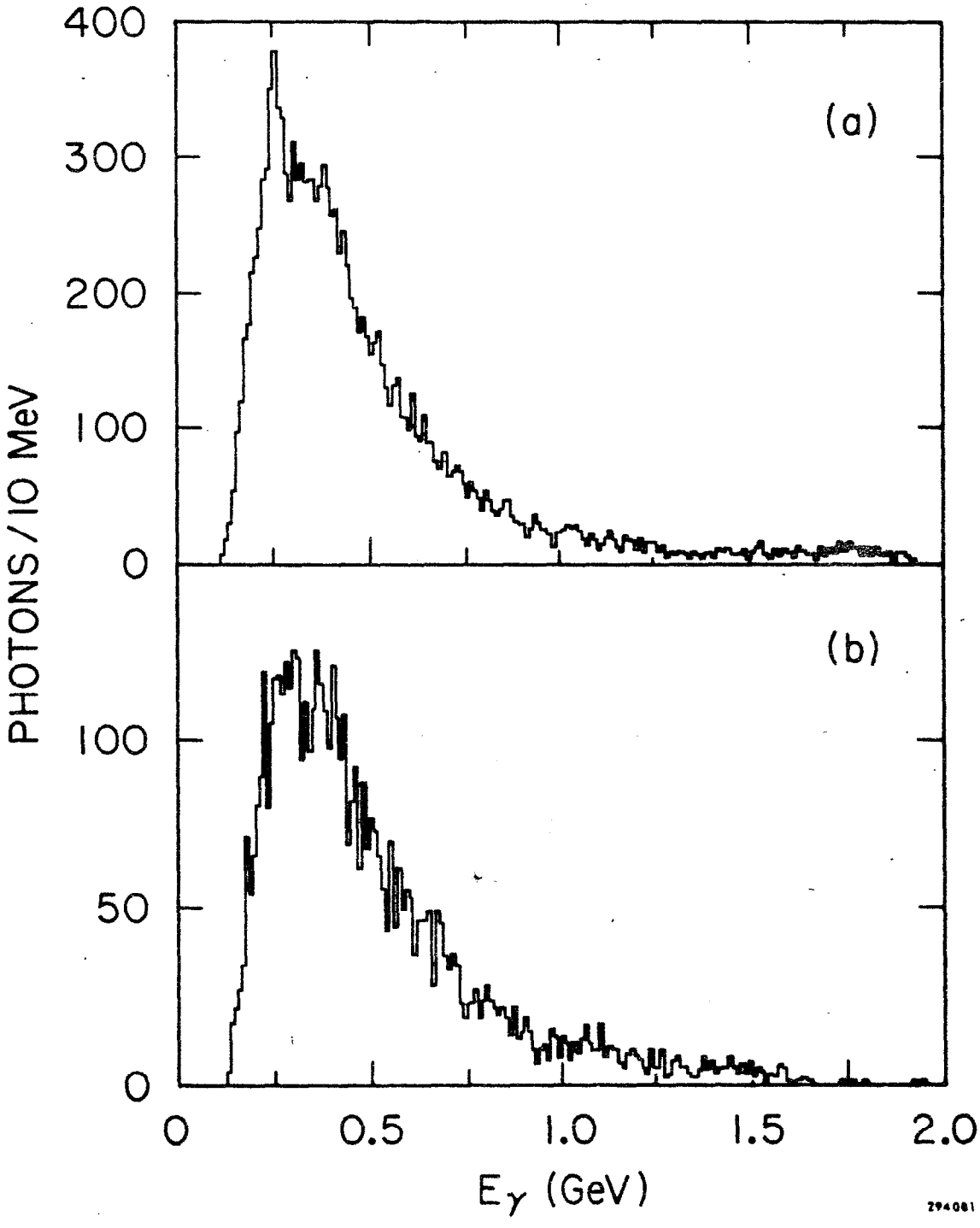
400
300
200
100
0
(a)
PHOTONS / 10 MeV
100
50
0
(b)
0
0.5
1.0
1.5
2.0
E_γ (GeV)
294081

Fig. 13

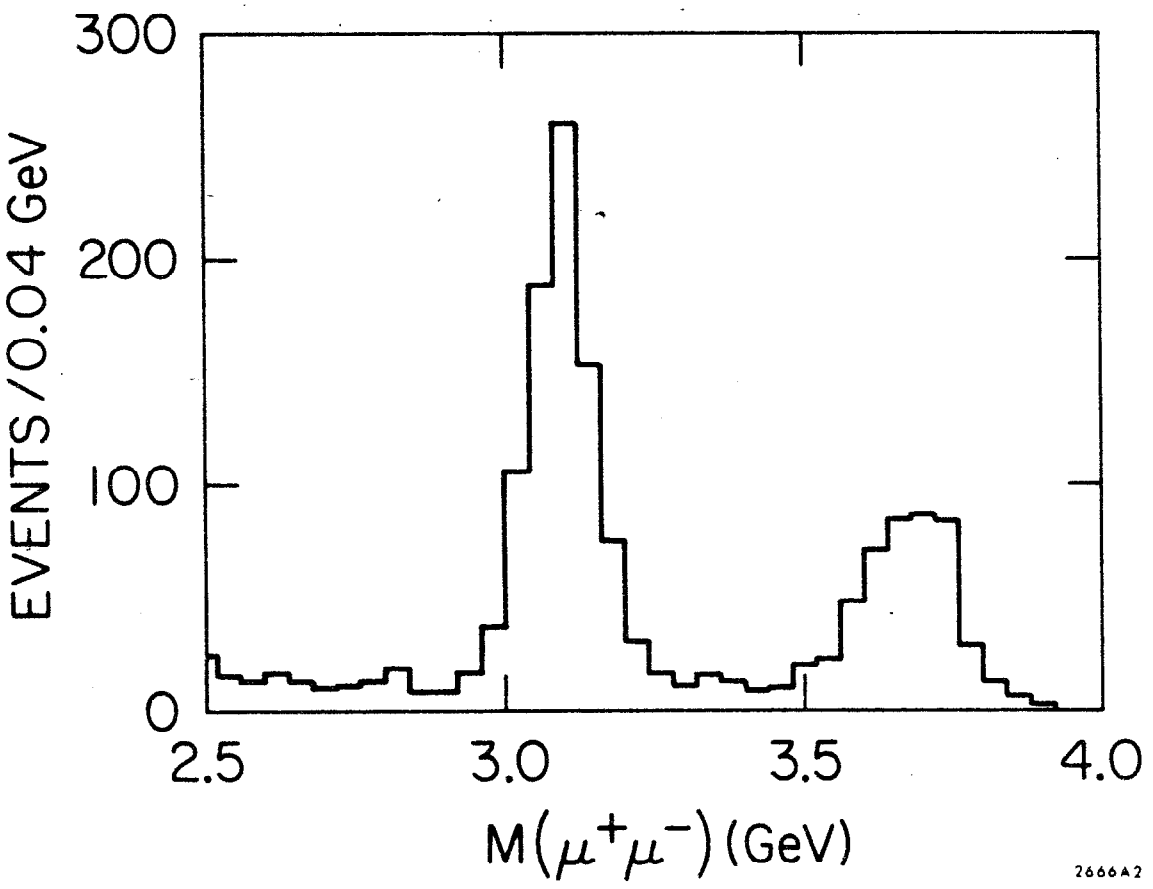

Fig. 14

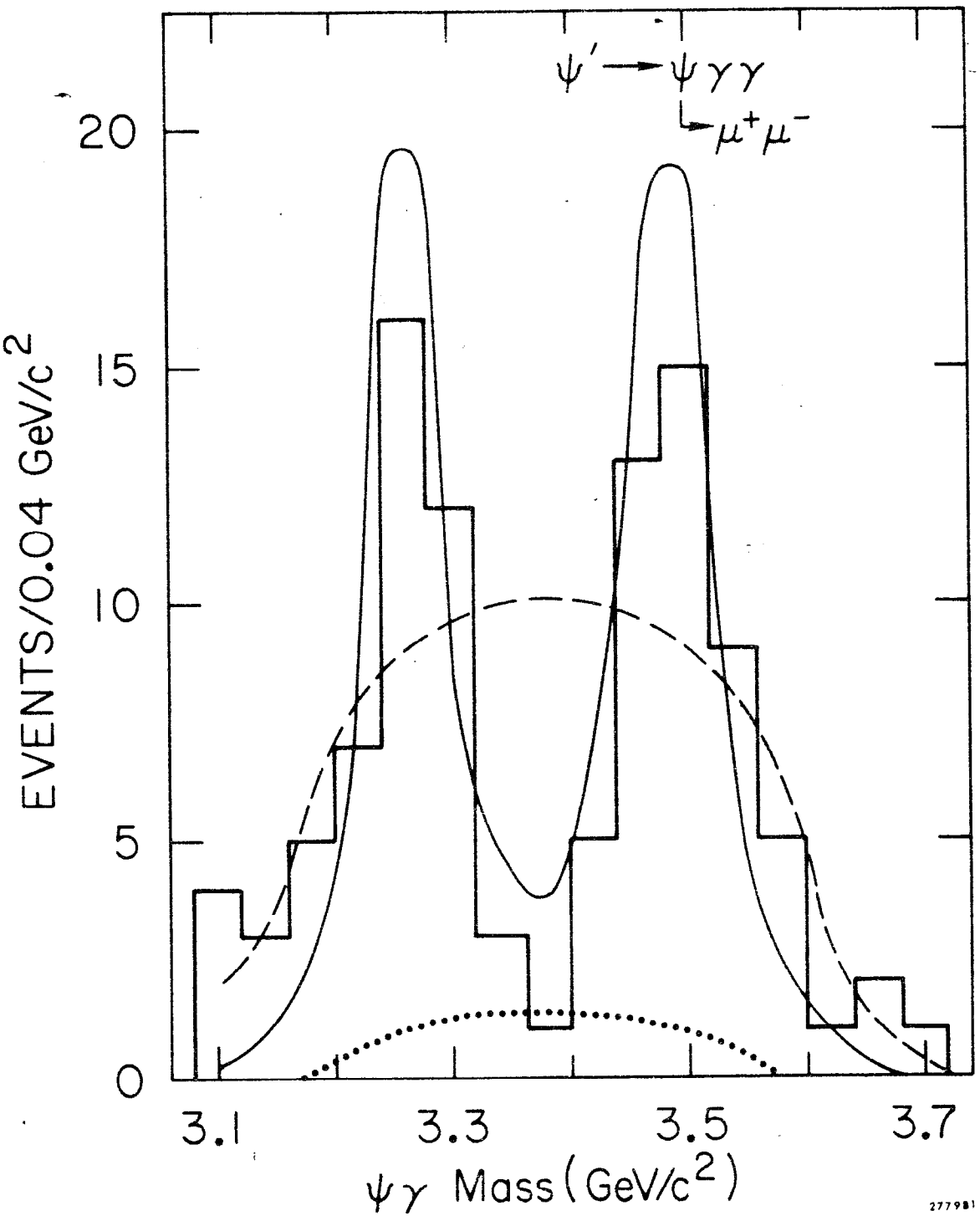
ψ′ → ψγγ
↳ μ⁺μ⁻
EVENTS/0.04 GeV/c²
20
15
10
5
0
3.1
3.3
3.5
3.7
ψγ Mass (GeV/c²)
277981

Fig. 15

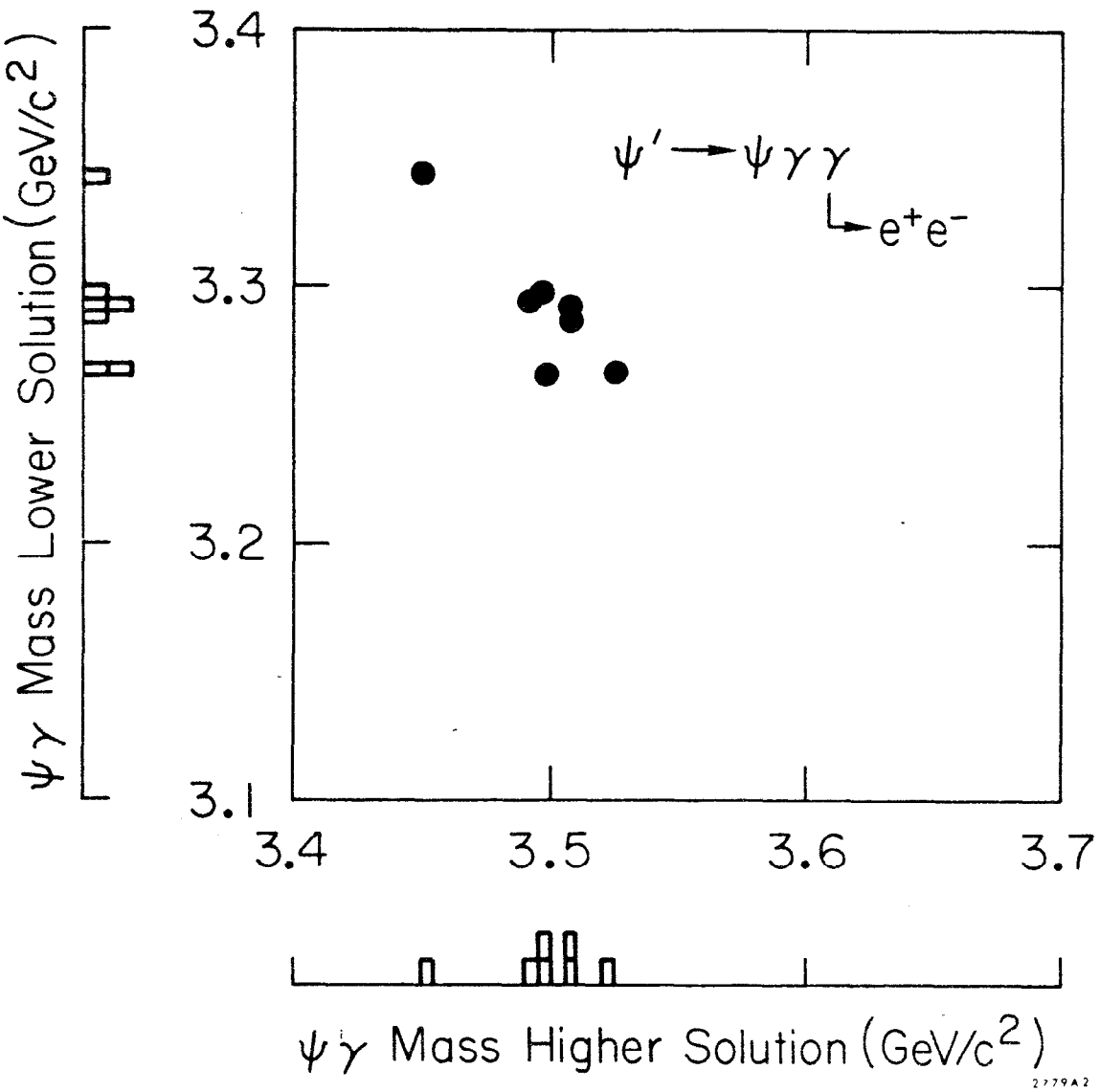
3.4
3.3
3.2
3.1
3.4
3.5
3.6
3.7
ψ′ → ψγγ
└→e⁺e⁻
ψγ Mass Lower Solution (GeV/c²)
ψγ Mass Higher Solution (GeV/c²)
2779A2

Fig. 16

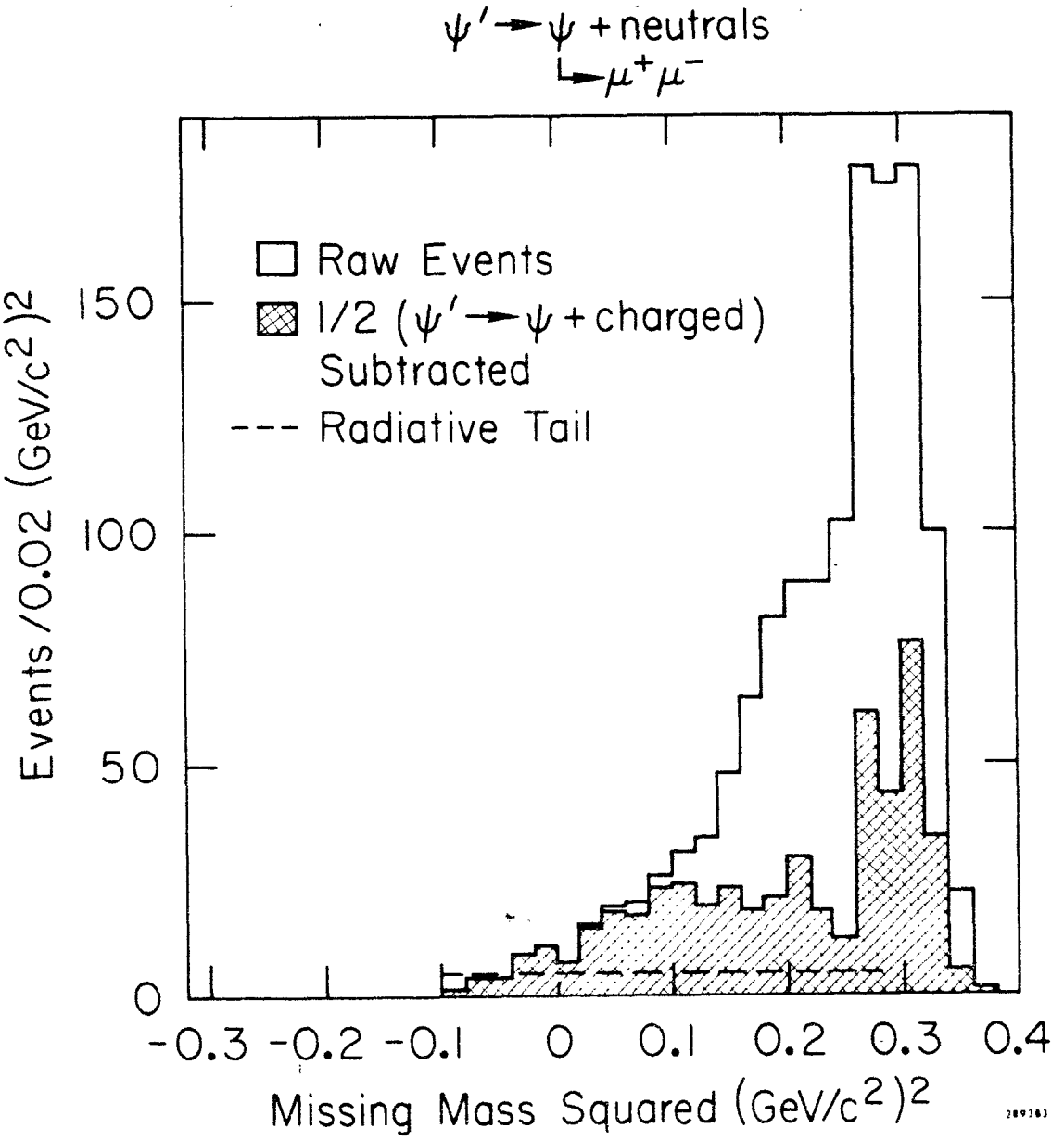
ψ′→ψ + neutrals
↳→μ⁺μ⁻
Raw Events
1/2 (ψ′→ψ + charged)
Subtracted
--- Radiative Tail
Events /0.02 (GeV/c²)²
150
100
50
0
-0.3 -0.2 -0.1 0 0.1 0.2 0.3 0.4
Missing Mass Squared (GeV/c²)²

Fig. 17

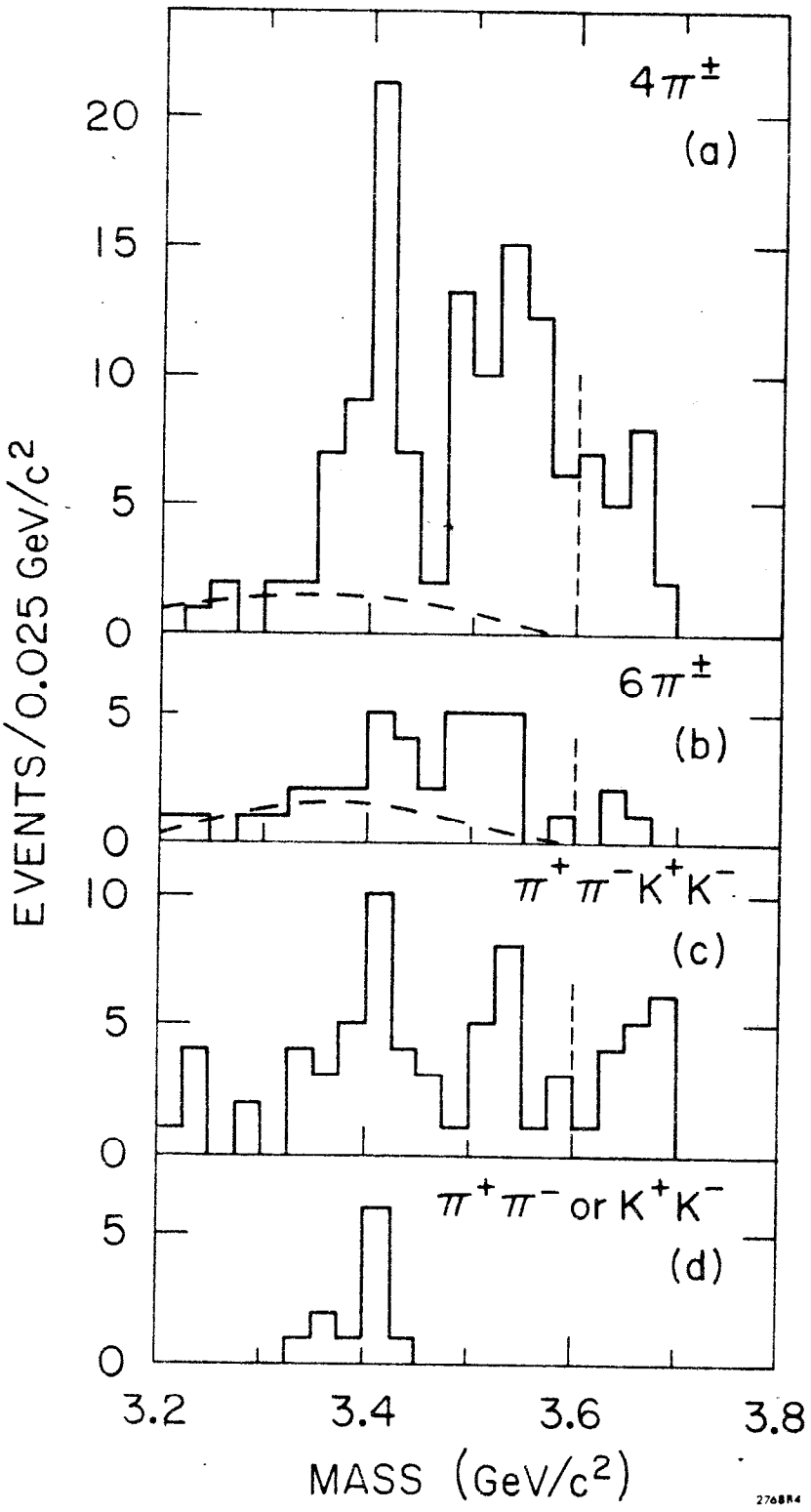
$4\pi^{\pm}$
(a)
$6\pi^{\pm}$
(b)
$\pi^+\pi^-K^+K^-$
(c)
$\pi^+\pi^-$ or K^+K^-
(d)
EVENTS/0.025 GeV/c²
MASS (GeV/c²)
3.2
3.4
3.6
3.8
0
5
10
15
20
2768R4

Fig. 18

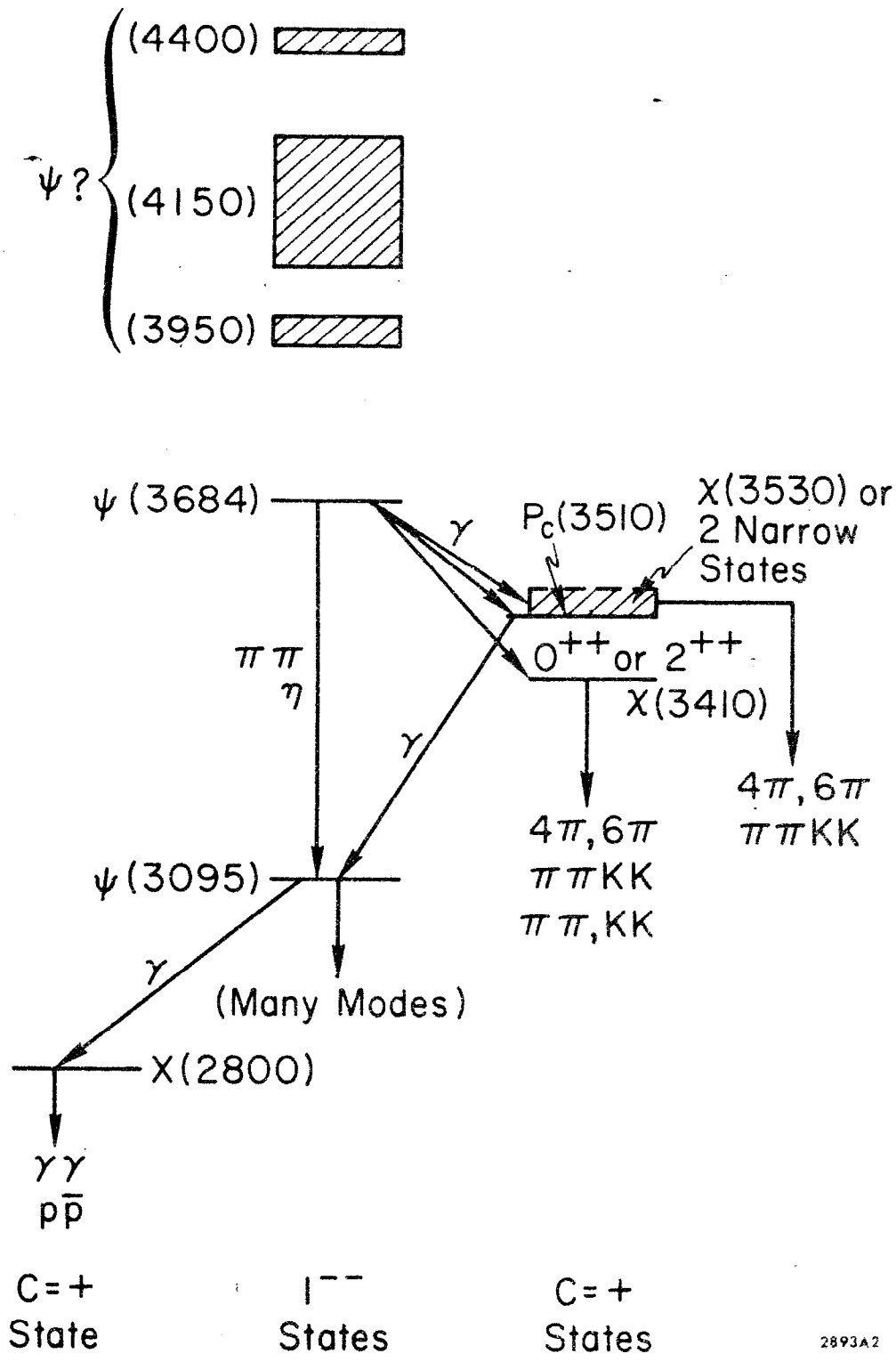
(4400)
ψ?
(4150)
(3950)
ψ(3684)
γ
Pc(3510)
χ(3530) or
2 Narrow
States
ππ
η
0++ or 2++
χ(3410)
γ
4π, 6π
ππKK
4π, 6π
ππKK
ππ, KK
ψ(3095)
γ
(Many Modes)
X(2800)
γγ
pp̄
C=+
State
1−−
States
C=+
States
2893A2

Fig. 19

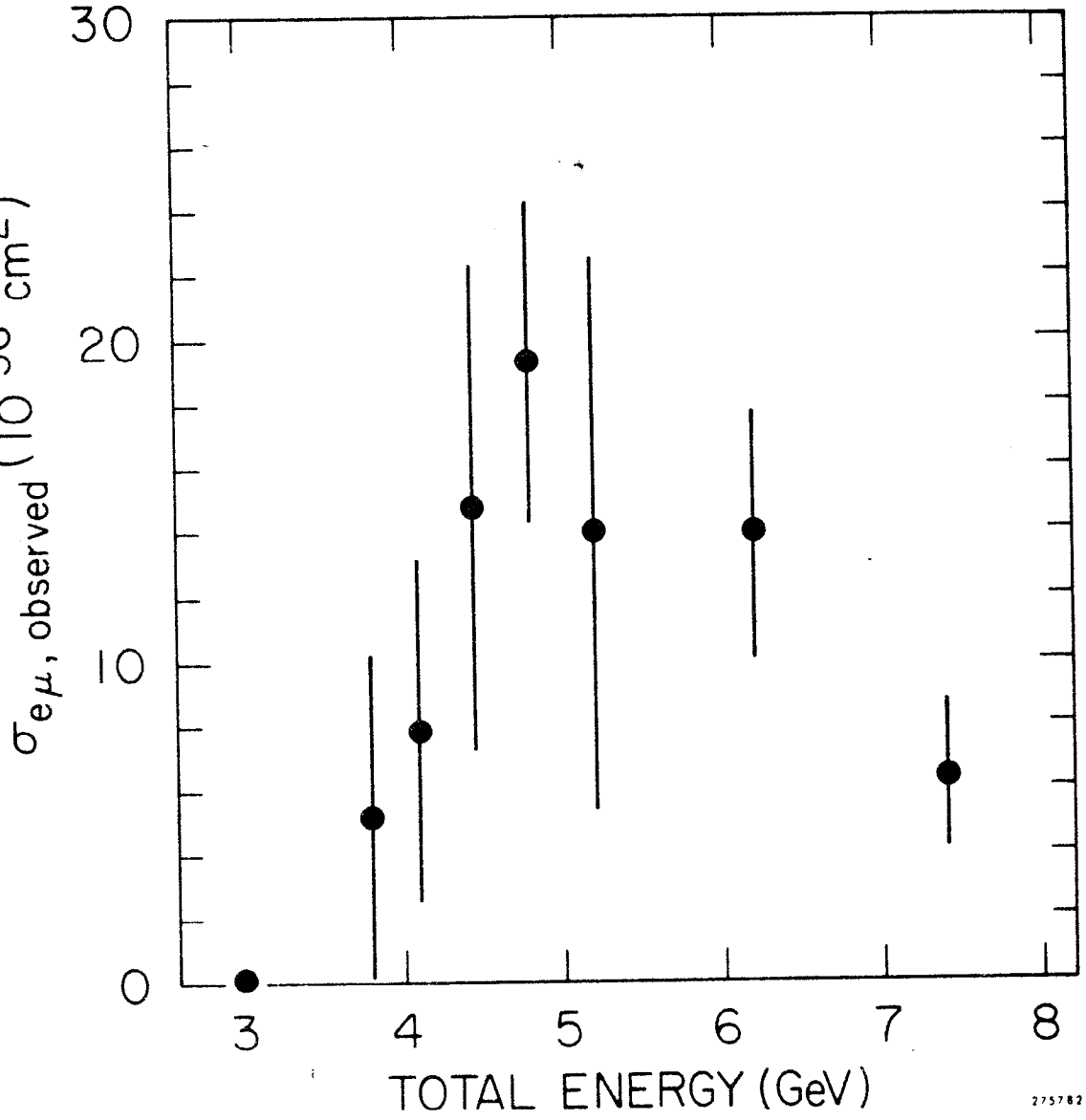
30
20
10
0
$\sigma_{e\mu}$, observed (10^{-36} cm^2)
3
4
5
6
7
8
TOTAL ENERGY (GeV)
275782

Fig. 20

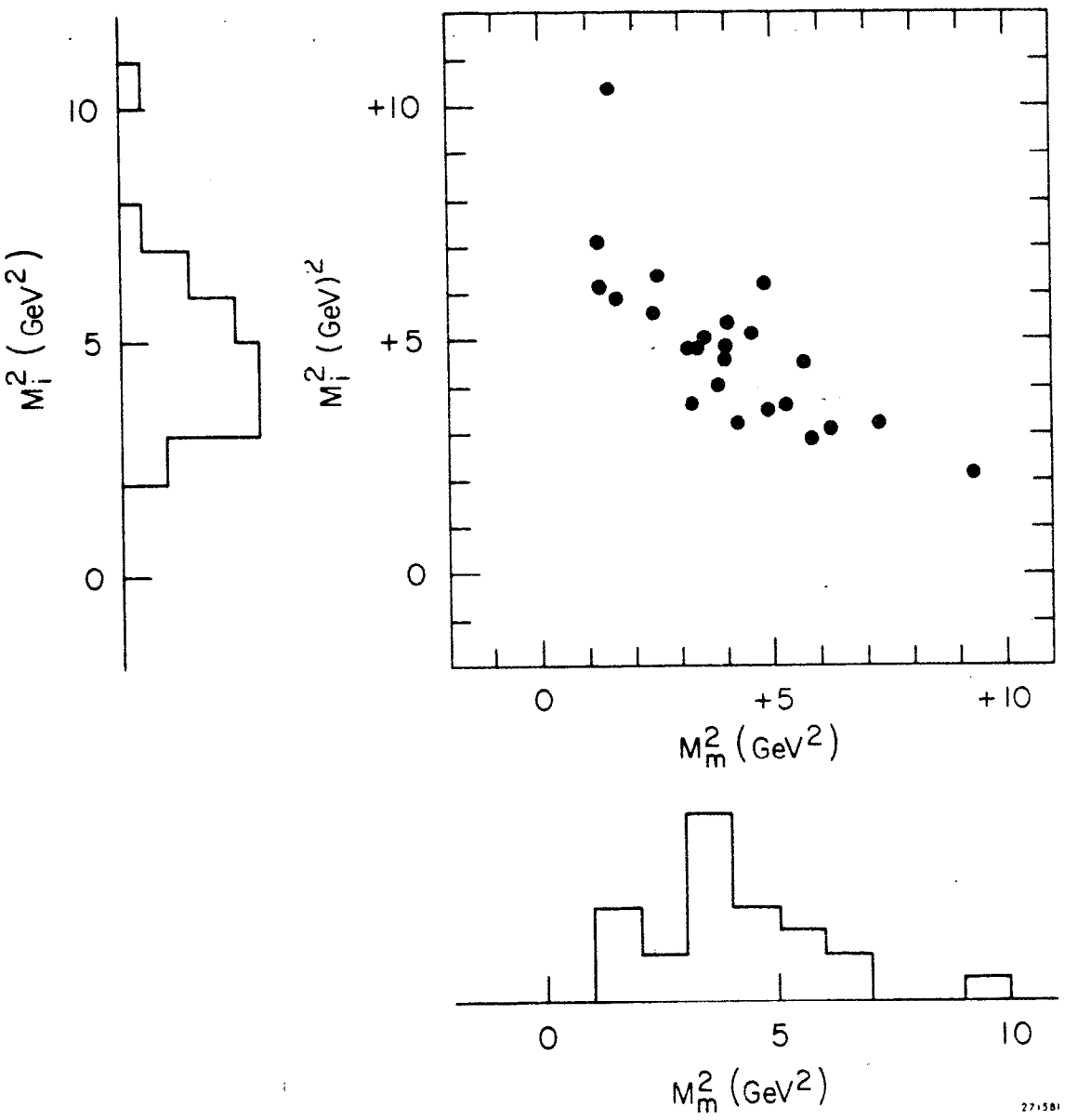

Fig. 21

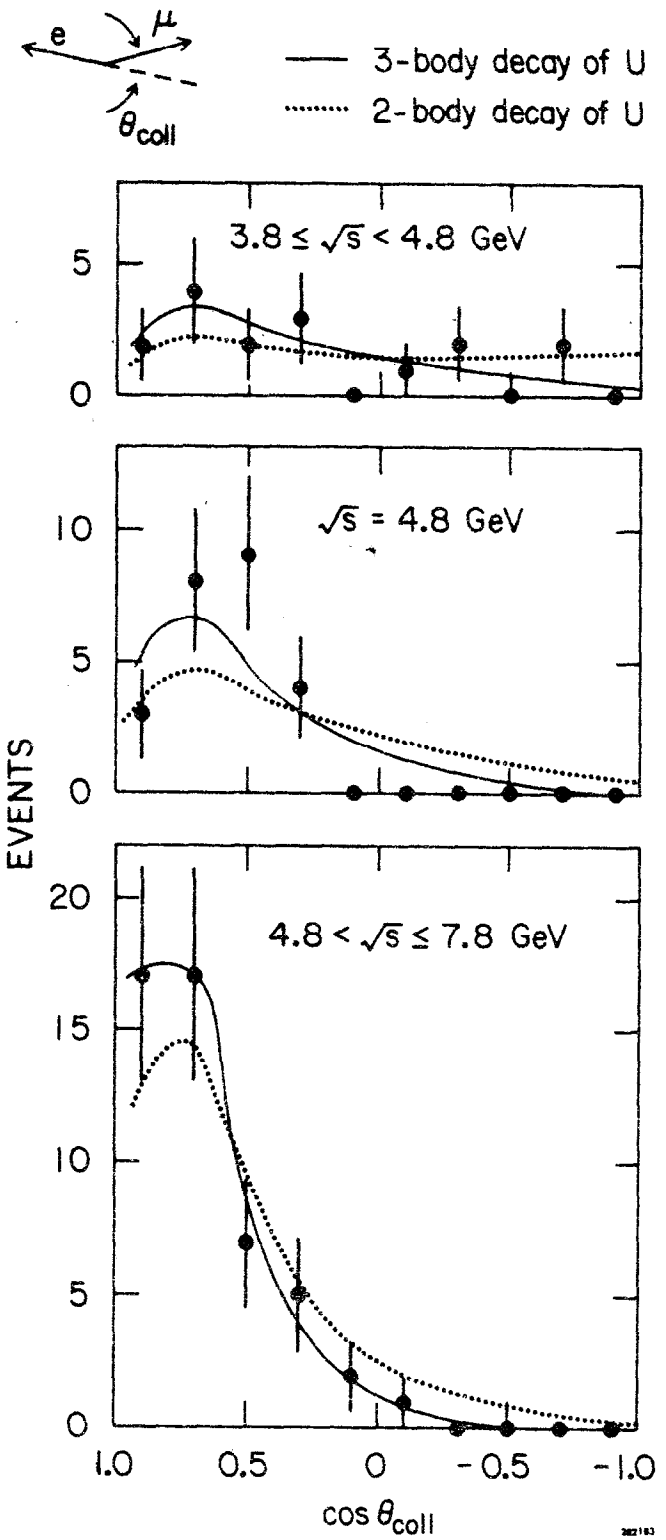
e
μ
θcoll
3-body decay of U
2-body decay of U
3.8 ≤ √s < 4.8 GeV
√s = 4.8 GeV
4.8 < √s ≤ 7.8 GeV
EVENTS
cos θcoll
1.0
0.5
0
-0.5
-1.0

Fig. 22

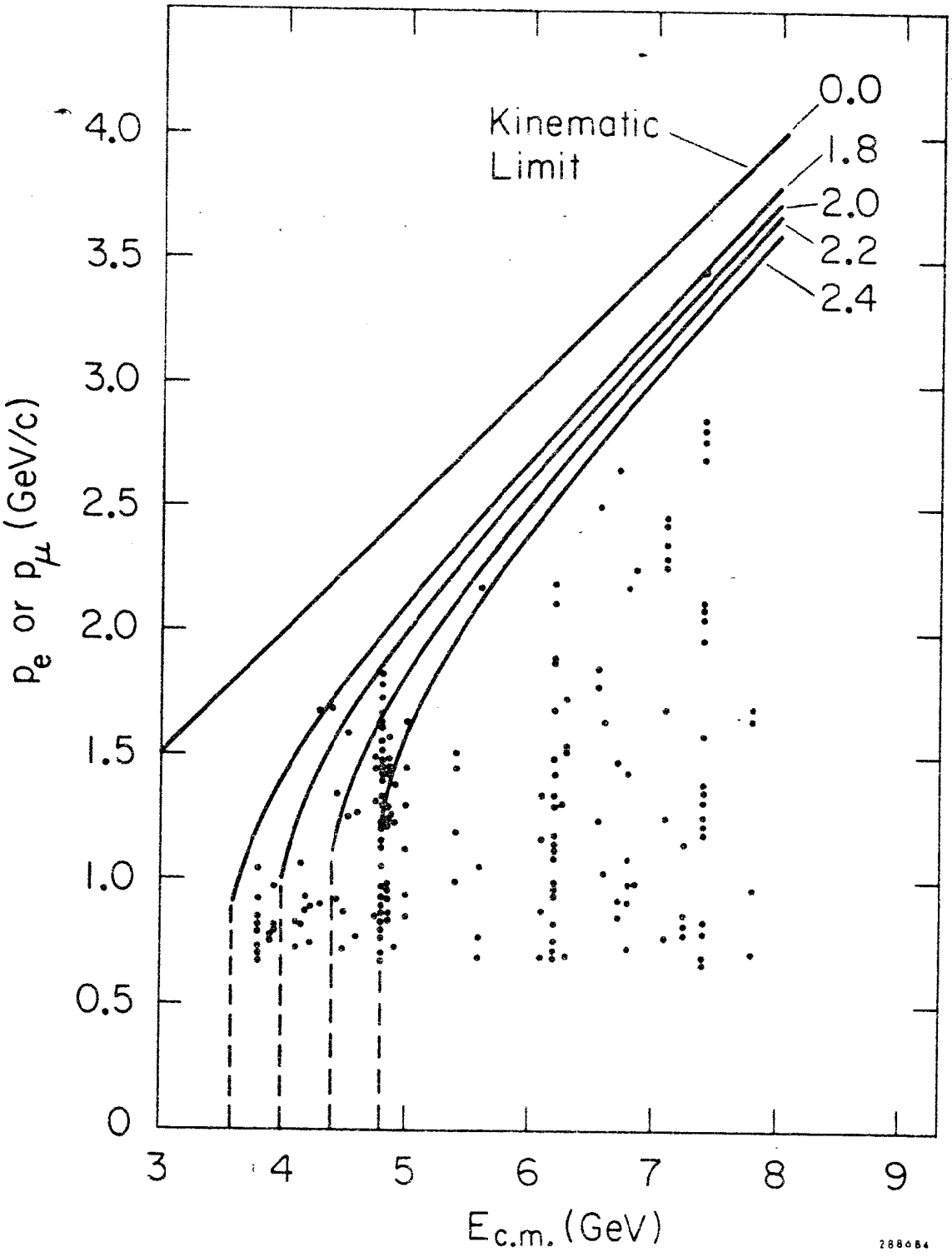
Kinematic
Limit
0.0
1.8
2.0
2.2
2.4
4.0
3.5
3.0
2.5
2.0
1.5
1.0
0.5
0
p_e or p_μ (GeV/c)
3
4
5
6
7
8
9
$E_{c.m.}$ (GeV)
288684

Fig. 23

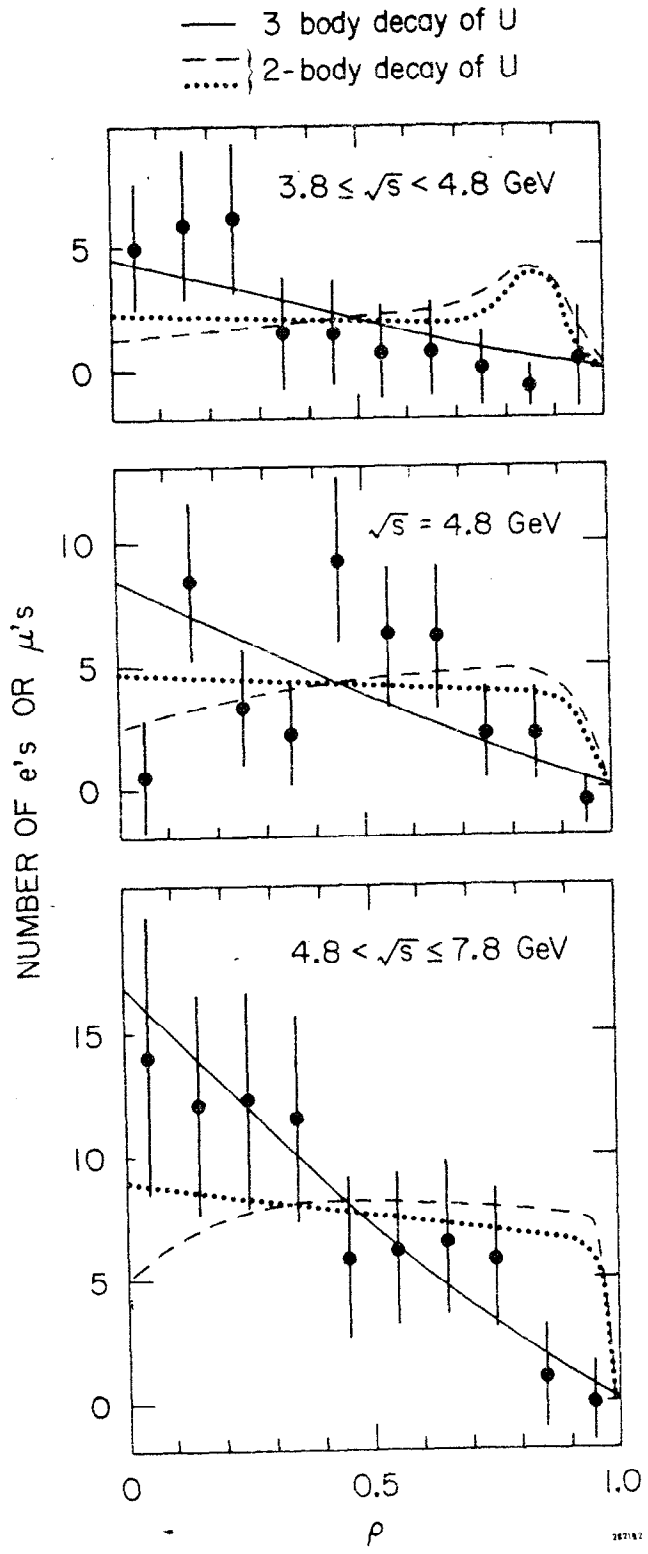
3 body decay of U
2-body decay of U
3.8 ≤ √s < 4.8 GeV
√s = 4.8 GeV
4.8 < √s ≤ 7.8 GeV
NUMBER OF e's OR μ's
ρ
0
0.5
1.0
5
10
15

Fig. 24